Doctoral Dissertation

Structure-based design of bioavailable streptavidin and biotin analogs aiming to establish pre-targeting cancer therapy

Tatsuya Kawato

January 2015

Department of Applied Chemistry

Graduate School of Engineering

Osaka University

Structure-based design of bioavailable streptavidin and biotin analogs aiming to establish pre-targeting cancer therapy

(がんのプレターゲティング治療の確立を目指した生体投与可能な
ストレプトアビジンとビオチン誘導体の構造に基づく分子設計)

2015

Tatsuya Kawato

Department of Applied Chemistry

Graduate School of Engineering

Osaka University

Preface

The work of this thesis has been carried out under the supervision of Professor Dr. Tsuyoshi Inoue at Department of Applied Chemistry, Graduate School of Engineering, Osaka University.

The object of this thesis is to create a practical and bioavailable streptavidin binding system for application to antibody pre-targeting method for cancer therapy.

The author wishes that a new streptavidin binding system provided in this study would be utilized for pre-targeting method as a novel delivery tool in the near future.

Tatsuya Kawato

Department of Applied Chemistry
Graduate School of Engineering
Osaka University
Suita, Osaka
Japan

January 2015

Contents

General Introduction

Cancer and antibody therapy

The recent advance in molecular biology has greatly improved our understanding of cancer dynamics, and has provided unexpected clues for designing effective cancer treatment. However, cancer remains to be a major public health problem and is a leading cause of death among men in many economically developed countries including Japan. More specifically, cancer accounts for 7.6 million deaths worldwide, and its mortality rate is predicted to increase, with an estimated 13.1 million cancer-related deaths in 2030 (*1-3*). Therefore, the development of caner therapies with greater effectiveness is in urgent need.

Traditional cancer chemotherapeutic drugs frequently cause serious side effects because they affect not only cancer cells, but also cells that are actively growing and dividing (*4, 5*). In addition, such side effects limit dose escalation, leading to incomplete tumor response and early relapse (*6*). Thereby, it is not surprising that the focus on cancer therapy has been dramatically shifted from traditional cytotoxic chemotherapy to target therapy, with an aim of killing cancer cells without affecting the growth of normal cells. Monoclonal antibodies are one of the most powerful tools for targeted cancer therapy because it allows treatment to target specific cells, causing less cytotoxicity to healthy cells (*4, 5, 7*). Antibodies produced by plasma cells can bind selectively to antigens that are overexpressed on the surface of cancer cells. In recent years, antibody-based cancer therapy has achieved considerable success and is now one of the standard strategies for cancer treatment (*8*).

History of Antibody-based cancer therapy

Targeted cancer therapy using monoclonal antibodies has a long history of over 100 years, with considerable efforts being devoted to its clinical application. In 1890, Shibasaburo Kitasato and Emil von Behring discovered that the serum of immunized animals contained substances that could bind to their relevant pathogens with high specificity (*9*). Since then, the term "antibody" was coined to describe substance with anti-microbial activity in the immune serum. After their discovery, the concept of specific recognition and elimination of cancer cells by antibodies was proposed by Paul Ehrlich in 1907, termed "magic bullet" theory of targeted therapy (*10*). The technology had a limited application at that time, because of its failure to produce identical antibodies specific to given antigens (*11*). After 70 years of endeavor, the vision finally became practical in 1975 with the development of one key method by Kohler and Milstein (*12*), namely "Hybridoma technology", which enables the production of monoclonal antibodies with single cancer specificity, and antibody cancer therapeutics has thereafter been developed rapidly (*13, 14*). Although the first generation of monoclonal antibodies had been limited in clinical use because of immunogenicity from their murine regions, the advent of chimeric, humanized and fully human monoclonal antibodies has overcome the barrier (*13-15*).

Antibodies can invoke tumor cell death by directly blocking ligand-receptor growth and survival pathways or inducing apoptosis (*7, 14, 16-18*). Additionally, antibodies also can kill cancer cells thorough immune-mediated cell killing such as antibody-dependent-cellular cytotoxicity (ADCC) or complement-dependent cytotoxicity (CDC) (*13, 16, 19*). The Fc fraction of antibody is of particular importance for mediating tumor cell killing through ADCC and CDC. For example, in ADCC, the antibody Fc fragment interacts with Fc receptor of the effector cells, such as natural killer (NK) cells and macrophages, and results in target cell phagocytosis, while in CDC, the binding of the antibody Fc region to complement component activates complement system to lyse the targeted cancer cell.

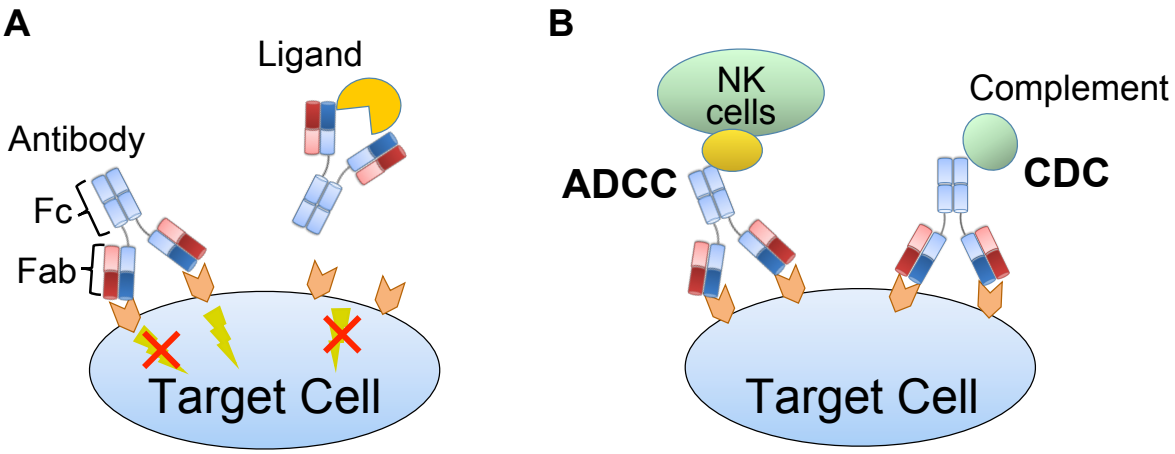

Fig. 1. Antitumor mechanisms of action of monoclonal antibodies.
(A) Inhibition of ligand-receptor growth and induction of apoptosis.
(B) ADCC and CDC.

Despite the great promise of antibody-based therapies, the therapeutic and cytotoxic activity of naked monoclonal antibody treatment yields various different outcomes, thus the potential applicability for this therapy is low (*15*). In an effort to improve the efficacy, a number of antibodies conjugated with radioactive isotopes or toxic agents, called "arming antibodies", have been developed and studied extensively (*5, 20-24*).

Radiolabeled antibodies

Radiolabeled antibodies are particularly attractive reagents for imaging and therapy of cancer treatment. Ideally, this approach delivers a high radiation does specifically to cancer cells using antibodies as delivery vehicles for radionuclides (Fig. 2). In clinical tests, Anti-CD20 monoclonal antibodies labeled with either ^{131}I or ^{90}Y, now known as ^{131}I-tositumomaba and ^{90}Y-ibritumomab approved by the U.S. Food and Drug Administration (FDA), were proved to be more efficacious in inducing remissions compared to the respective naked antibodies, and also appear to be more

effective than the prior course of therapy, such as chemotherapy (*25-27*). The efficacy of radiolabeled antibody therapy has been reviewed elsewhere (*28-32*).

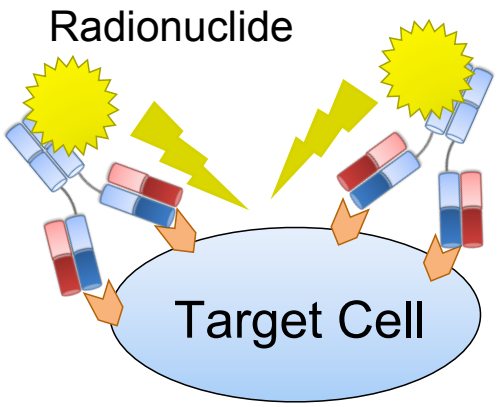

Fig. 2. Antitumor mechanism of radiolabeled antibodies.

However, these conjugated antibodies clear very slowly from blood and exhibit slow extravasation and diffusion efficacy to tissues probably due to its large size (~150 kDa). The prolonged circulation of direct-radiolabeled antibodies for maximal accumulation in tumors results in high levels of background radioactivity and toxicity in normal tissues and blood (*33*). Therefore, to avoid treatment-related morbidity and mortality, the radiation dose delivered to neoplastic masses is kept as low as possible. As a result of dose-limiting toxicities, patients treated with conventional direct-radiolabeled antibodies eventually relapse after favorable initial response (*24, 34, 35*). In order to circumvent this problem, a number of strategies have been undertaken to enhance the tumor-to-background ratio of delivered radioactivity. To this end, multistep "pre-targeting" method has proved superior to direct-radiolabeled antibodies.

Pre-targeting cancer therapy using Streptavidin/Biotin interaction

The principle of pre-targeting method involves the separate administration of antibody and a radionuclide carrier (*36, 37*). In this method, the unmodified antibody is given as a first injection until

it reaches the maximum level, followed by delivery of radionuclide agent recognizable by antibody. This can optimize delivery of the therapeutic radionuclide to cancer cells, while preventing normal tissues from systemic exposure to harmful effects of radiation (*38*). The pre-targeting procedure using the streptavidin/biotin system has received much attention and been already validated by several preclinical studies (*27, 37, 39-45*).

Streptavidin (SA) is a homotetrameric protein from *Streptomyces avidini*, while biotin (BTN) is a vitamin widely distributed in mammalian tissues (Fig. 3). It is well documented that each monomer of SA binds one BTN with exceptional high specificity and strong affinity ($K_d = 10^{-14}$–10^{-15} M) (*46, 47*), thereby this SA/BTN binding system has been employed as various biotechnological tools, such as the labeling and binding experiments (*48-51*).

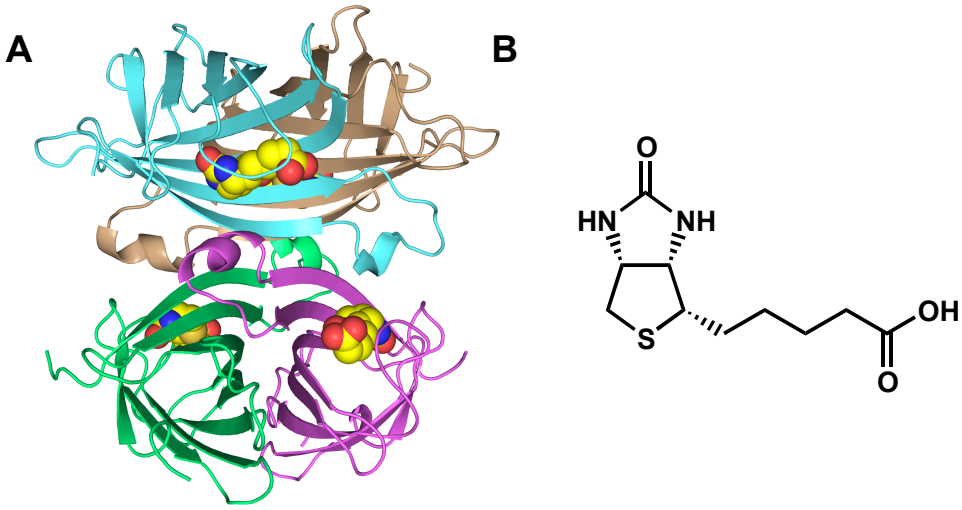

Fig. 3. (A) Structure of SA (PDB ID: 3WYQ). (B) Structural formula of BTN.

This high binding affinity makes the SA/BTN interaction an ideal tool for pre-targeting method; although other pre-targeting methods comprising a bispecific monoclonal antibody/hapten and an oligonucleotide/antisense have also been proposed (*39, 52*). In the pre-targeting method with SA/BTN system, SA prefused with a single chain antibody fragment (Fab or ScFv) is injected into patients and allowed to localize in cancer cells, followed by the clearing of excessive SA-antibody conjugates

through liver by an appropriately designed clearing agent. A radiolabeled biotin derivative is then administered systemically, whereupon it is either captured by streptavidin localized at tumors, or is rapidly cleared through urine via the kidneys (Fig. 4) (*53*). Anti-CD40 or anti-CD20 antibodies with streptavidin have shown that this method dramatically increases the tumor-to-normal organ ratio of delivered radioactivity (*33, 54*). It dramatically increased the tumor-to-normal organ ratio of delivered radioactivity by 10- to 100-fold (16–18). Despite encouraging preliminary studies, the clinical application of SA/BNTN has not yet been achieved because there exist twt major issues regarding the use of SA/BTN system in human body.

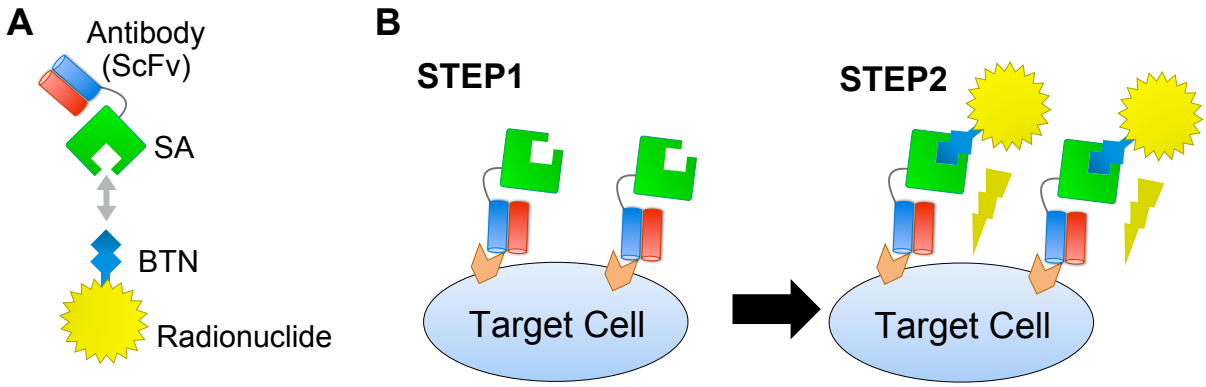

Fig. 4. Pre-targeting method using SA/BTN interaction.
(A) Illustration of SA-fused ScFv and radiolabeled BTN. (B) Schematic illustration of the pre-targeting method.

Two problems of SA/BTN interaction

One major drawback limiting its application is the immunogenicity arising from the bacterium-derived SA, which results in the production of anti-SA antibodies, thereby reducing the concentration of SA in the serum and lowering the efficacy of SA/BTN binding system, thus precluding its long-term usage in the human body (*27, 53, 55, 56*). Meyer *et al.* reported the development of SA mutant with lowered immunogenicity by substituting specific charged and aromatic amino acid residues, which make up putative conformational epitopes for interaction with B

cells (*53*). The substitutions, however, also increased the destabilization of tetrameric assembly and the dissociation rate from BTN probably due to the replacements mainly with Ala or Gly. Recently, Kodama *et al.* succeeded in synthesizing a low immunogenic SA mutant, termed LISA-314, by introducing six amino acid residues (Y22S/Y83S/R84K/E101D/R103K/E116N) at locations of wild-type SA (SA-WT) that were proposed to be involved in its immune recognition. LISA-314 has greatly decreased immunoreactivity against monkey antiserum while retaining biophysical properties including biotin binding and thermal stability. The design focused on reducing reactivity against anti-SA-WT serum and the number of *in silico* T-cell epitopes. Rather than simply mutating the residues to neutral amino acids like Ala and Gly, residues evading immunogenic recognition while preserving the electrostatic charge and functional moiety are of considerably higher priority for the mutational design.

The second problem is the presence of competing endogenous BTN species in serum and tissues, whose concentrations are great enough to block the BTN-binding sites of SA (*57, 58*) before the exogenous radiolabeled BTN derivative can bind to the target site, resulting in a dramatic reduction of the efficacy of pre-targeting method. Reznik *et al.* developed a SA mutant that shows slightly higher affinity for a biotin analog, iminobiotin (IMN) than BTN (*59*). Hamblett *et al.* prepared a SA mutant that has a reduced affinity for BTN because of the faster dissociation, and a bivalent BTN showed a higher affinity to the mutant than monovalent BTN, allowing the exchange of pre-bound endogenous BTN species with the bivalent BTN molecule (*60*) (*61*). Despite the great progress of SA mutant, no practical SA mutant with absolute zero affinity for natural BTN species has been made so far. To maximize the efficacy of pre-targeting method, the development of a novel SA-binding system overcoming the abovementioned issues is needed.

Contents of this thesis

This thesis aims to provide a practical and bioavailable SA-binding system for the application to pre-targeting method by a consideration and improvement of LISA-314. The author developed a modified LISA-314 binding system that selectively binds to an artificial biotin analog with high affinity by molecular design based on X-ray structural analysis.

In chapter 1, the effects of six substitutions on the three-dimensional structure and protein function in LISA-314 were evaluated by determining its high-resolution crystal structure. Unlike previous strategies, which mainly used alanine or glycine, the substitutions toward LISA-314 were designed to preserve the electrostatic charge and functional moieties of the SA-WT residues. However, it is not confirmed whether these characteristics are really maintained after introducing the mutations. Structural information of LISA-314 is thus necessary not only for this verification but also for the molecular design in order to solve the second problem. The results demonstrated that the overall structure and the BTN binding site are completely identical to those of SA-WT. Effects of substitutions are limited to around the side chains of the substituted residues.

Chapter 2 describes the development of the modified LISA-314 binding system without being affected by endogenous BTN species that block the binding sites of LISA-314 and interfere the binding of exogenous biotin-labeled drugs. To achieve this aim, three amino acid substitutions were introduced in the binding pocket of LISA-314. The resultant mutant, namely V212, binds to a non-natural biotin analog (IMNtail) selectively (K_d = 5.9×10^{-7} M), while it shows no affinity for biocytin.

In chapter 3, in order to increase the affinity between V212 and IMNtail, a bivalent biotin analog was designed by connecting two IMNtail molecules. The bivalent analog, namely Bis-IMNtail, showed much higher affinity for V212 (K_d = 8.3×10^{-10} M) than monovalent IMNtail by inducing avidity effect. The crystal structure of V212 complexed with Bis-IMNtail was also determined.

Chapter 1

Crystal structure of a streptavidin mutant with low immunogenicity

1.1 Introduction

As mentioned in General Introduction, pre-targeting method based on streptavidin (SA)/biotin (BTN) interaction, which has extremely high affinity (K_d = 10^{-14}–10^{-15} M) (*46, 47*), holds great promise for targeted cancer therapy (*27, 37, 39-45*). For its application, a Low Immunogenic SA mutant No. 314 (LISA-314) has been created recently by replacements of six amino acid residues (Y22S/Y83S/R84K/E101D/R103K/E116N) in core wild-type SA (SA-WT) (*62, 63*).

In this chapter, the author determined the high-resolution crystal structure of LISA-314 and evaluated the effect of substitutions inside LISA-314 on the protein function and the three-dimensional structure.

1.2. Material and methods

1.2.1. Expression and Purification

The core SA-WT and LISA-314 were cloned into cleavable eXact tag fusion pPAL7 vector (Bio-Rad Laboratories). For the expression, SA-WT and LISA-314 plasmids were transformed into the *Escherichia coli* BL21Star(DE3) strain, which was cultivated in Luria-Broth medium supplemented with 100 μg/mL ampicillin at 37 °C. When the optical density (λ = 600 nm) reached a value of 0.5, 0.4 mM isopropyl-β-D-thiogalactopyranoside (IPTG) was added for induction. Cultivation was continued for approximately 24 h at 16 °C. Cells were harvested by centrifugation at

4 °C at 8,000 × g for 20 min and resuspended in extraction buffer (10 mM phosphate, 100 mM NaCl, Complete EDTA-free protease inhibitor cocktail tablets (Roche) and Benzonase (Novagen) at pH 7.2). The sample was lysed by passing through a French press twice at 12,000 lb/in2. The lysate was centrifuged at 10,000 × g for 30 min to remove the insoluble fraction. The supernatant was loaded onto a HiTrap SP HP (GE Healthcare) and eluted with a linear gradient of 0.1–1.0 M NaCl in 10 mM phosphate buffer at pH 7.2. The eluted protein was dialyzed against binding buffer for the eXact column (Bio-Rad Laboratories) containing 10 mM phosphate and 300 mM sodium acetate at pH 6.8. The sample was then loaded onto an eXact column and the column was washed with the binding buffer. The column was further washed with the binding buffer supplemented with 100 mM NaF and incubated to allow cleavage of the eXact-tag at 25 °C for 1 h. The cleaved protein was collected in the flow-through and dialyzed against 10 mM phosphate buffer at pH 6.0 for SA-WT and pH 6.8 for LISA-314. The sample was loaded onto a hydroxyapatite column and eluted with a phosphate gradient (Bio-rad Laboratories). The eluted protein was buffer-exchanged into gel-filtration buffer (150 mM Tris-HCl and 150 mM NaCl at pH 7.5) using a Vivaspin 30-kDa cutoff (GE Healthcare). BTN was added to the sample at excess molar ratio for the SA-WT or LISA-314. Further purification was carried out by gel-filtration chromatography using a HiLoad 26/600 Superdex 75 column (GE Healthcare). The purified sample was then concentrated to approximately 9.0 mg/mL, estimated by the absorbance at 280 nm.

1.2.2. Crystallization

Crystallization was performed by the sitting-drop vapor-diffusion methods at 20 °C in Violamo 96-well plates (As One, Osaka, Japan). Sixty microliters of the reservoir solution was added to each well of the 96-well plates. Crystals of SA-WT were obtained by mixing 0.5 μL of protein solution

(9.0 mg/mL SA-WT, 150 mM Tris-HCl and 150 mM NaCl at pH 7.5) and 0.5 μL of reservoir solution (0.2 M ammonium sulfate, 0.1 M sodium acetate trihydrate and 24%(w/v) PEG4000 at pH 5.2). On the other hand, crystals of LISA-314 were prepared by mixing 0.5 μL of protein solution (9.0 mg/mL LISA-314, 150 mM Tris-HCl and 150 mM NaCl at pH 7.5) and 0.5 μL of reservoir solution (0.2 M ammonium sulfate, 0.1 M sodium acetate trihydrate and 24%(w/v) PEG4000 at pH 5.2). Crystals were cryoprotected by the reservoir solution containing 30% glycerol.

1.2.3. X-ray data collection and processing

All datasets were collected on the beamline BL44XU at SPring-8 (Harima, Japan) under -173 °C. Data were indexed and scaled with the programs *DENZO* and *SCALEPACK* from the *HKL2000* program suite (HKL Research). The structures were solved by the molecular replacement with the program *Phaser* (*64*) from the *CCP4i* package (*65*) using a core streptavidin structure (PDB ID: 2F01) as the search model. The resultant structures were manually modified to fit into the experimental electron density maps, using the program *Coot* (*66*), then refined with the program *Refmac* (*67*) from the *CCP4i* package. The results of the structural analysis are summarized in Table 1-1. Figures were prepared with *Pymol* (http://www.pymol.org/). The final structure coordinates and structure factor amplitudes were deposited into the Protein Data Bank with IDs 3WYP for SA-WT and 3WYQ for LISA-314.

Table 1-1. Data collection and refinement statistics

	SA-WT	**LISA-314**
Data collection		
Space group	$P2_1$	$C2$
Unit-cell parameters (Å, °)	a = 50.35, b = 97.70, c = 52.57, β = 112.29	a = 63.22, b = 67.07, c = 56.36, β = 116.68
Wavelength	0.90000	0.82000
Resolution (Å)	50-1.30 (1.32-1.30)	50-1.00 (1.04-1.00)
R_{sym} (%)[a]	4.6 (34.5)	4.7 (29.6)
Total reflections	328,787	460,563
Unique reflections	110,519 (5,392)	107,216 (10,169)
$I/\sigma(I)$	23.4 (2.9)	30.7 (3.6)
Completeness (%)	96.0 (93.3)	95.4 (91.6)
Redundancy	3.0 (2.7)	4.3 (3.2)
Refinement		
Resolution	1.30	1.00
No. of reflections	104,885	101,796
R_{work} (%)[b]/R_{free} (%)[c]	13.1/17.9	13.7/16.3
No. of atoms		
Protein	3,697	1,805
Ligand/ion	136	109
Water	480	254
B factors		
Protein	9.2	8.4
Ligand/ion	16.3	18.5
Water	29.3	28.1
R.m.s deviations		
Bond length (Å)	0.025	0.026
Bond angles (°)	2.23	2.43
Ramachandran plot		
Favored (%)	95.30	96.04
Allowed (%)	3.42	3.52
Outliers (%)	1.28	0.44
PDB IDs	3WYP	3WYQ

Values in parentheses are for the highest-resolution shell

[a] R_{sym} is calculated as $\Sigma_{hkl}\Sigma_i|I_i(\text{hkl}) - \langle I(hkl)\rangle|/\Sigma_{hkl}\Sigma_i I(hkl)$, where $I_i(hkl)$ is the intensity of an individual measurement of the reflection with Miller indices hkl and $\langle I(hkl)\rangle$ is the average intensity from multiple observations.

[b] $R_{work} = \Sigma_{hkl}||F_{obs}| - |F_{calc}||/\Sigma_{hkl}|F_{obs}|$, where F_{obs} and F_{calc} are the observed and calculated structure-factor amplitudes, respectively.

[c] R_{free} is computed in the same manner as R_{work} but using only a small set (5%) of randomly chosen intensities that were not used in the refinement of the model.

1.3. Results and Discussion

1.3.1 Overview of the structure of LISA-314

Many structural analyses of SA have been reported previously (*68-73*). To perform a detailed structural comparison between LISA-314 and SA-WT, their high-resolution crystal structures in complex with biotin were determined by using the same protein expression, purification, and crystallization conditions (Table 1-1). In the asymmetric unit, two protomers are contained in LISA-314 and four in SA-WT.

LISA-314 forms a tetramer in a similar manner to SA-WT (Fig. 1-1A). Each subunit consists of an eight-stranded β-barrel with a ligand binding site at one end of the barrel. The root mean squared deviation (RMSD) value for the Cα carbon atoms of the whole structure between LISA-314 and SA-WT is calculated to be 0.70 Å, but the RMSD value for each protomer is actually calculated to be lower (0.50–0.70 Å). Except for part of the C-terminal region, the main chains of the protomer in LISA-314 superimpose well with those in SA-WT, even at substituted sites (Fig. 1-1B).

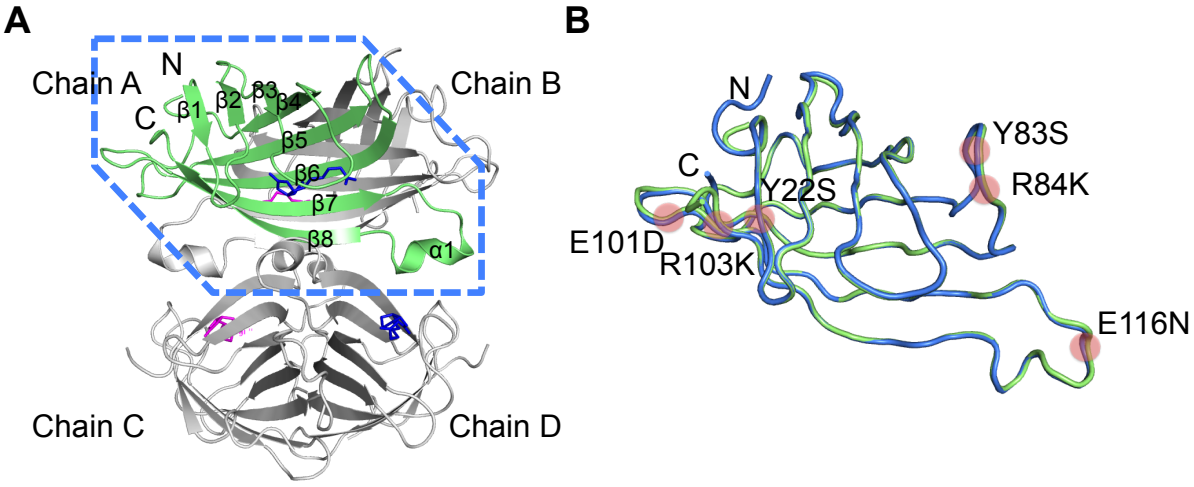

Fig. 1-1. Crystal structures of SA-WT and LISA-314.
(A) The overall structure of SA-WT depicted in ribbon diagram. In the tetramer, one of the protomers is shown in green, and the other three protomers are shown in gray. In the four protomers, 2 BTN (shown in blue) and 2 biotin-D-sulfoxide (shown in masenta) molecules are bound in the active sites. (B) Main chain tracing for SA-WT (green) and LISA-314 (blue) after superposition on protomer. Substituted residues are shown by a red circle.

1.3.2. The BTN-binding mode of LISA-314

In 2/4 protomers of SA-WT, the sulfur atom of BTN is oxidized, so the BTN-binding mode of LISA-314 was compared with the other 2/4 chains of SA-WT containing non-sulfoxide BTN. The sulfoxide form of BTN is sometimes seen in the crystal structure of the SA-BTN complex, even though it was not added in purification or crystallization step (*74, 75*). The BTN-binding mode of LISA-314 is the same as that of SA-WT, showing that the RMSD value for the BTN molecule between SA-WT and LISA-314 is only 0.05 Å. The BTN molecule was stabilized by an extensive network of hydrogen bonds and van der Waals interactions as is seen in SA-WT (Fig. 1-2).

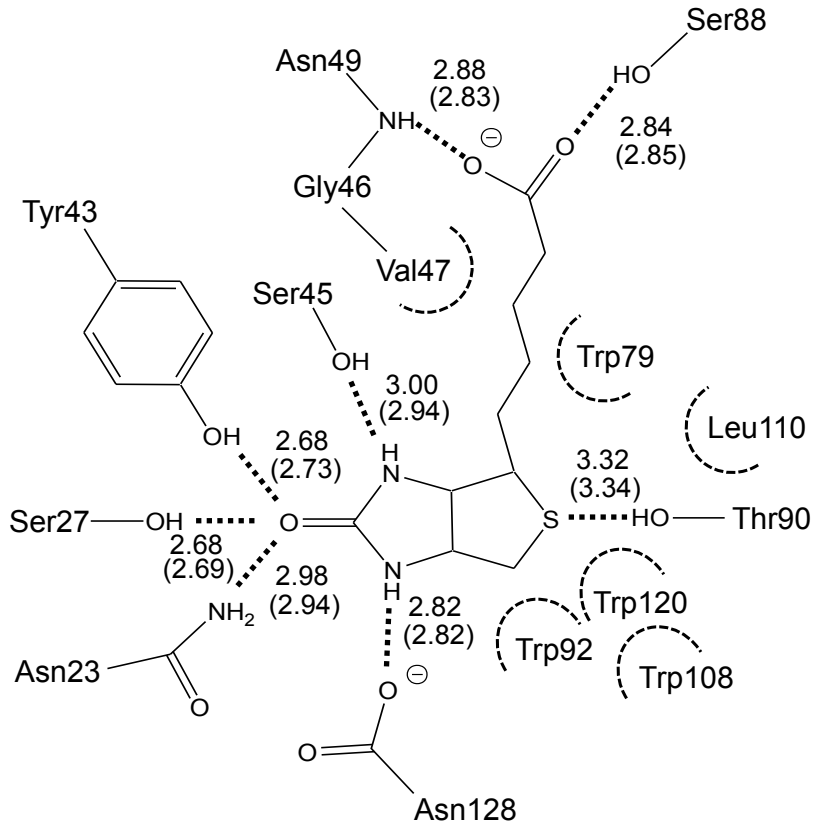

Fig. 1-2. Schematic representation of the interactions between BTN and LISA-314 or SA-WT. Dashed lines represent hydrogen bonds. The distances (Å) between residues of LISA-314 or SA-WT (parentheses) and BTN are shown.

1.3.3. Conformational changes at substituted sites and *B* factors

The structural change at every substitution site is summarized in Fig. 1-3, and the change of temperature (*B*) factors for all Cα carbon atoms is shown in Fig. 1-4. The *B* factor reflects the local mobility of protein backbones. Significant increases for *B* factors, which were not caused by packing effect, were observed around the substitution sites of Y83S and R84K. The electron density maps for the side chain of Y83 of SA-WT and S83 of LISA-314 are well ordered, and main chains near the residues are well superimposed (Fig. 1-3B). However, the hydrogen bond between R84 and N49, which was found in SA-WT, was broken owing to the substitutions of R84K and Y83S in LISA-314 (Fig. 1-3C), and the *B* factors of the residues around these substituted residues were increased (Fig. 1-4). In all the substitutions, a slight decrease in *B* factor was only observed by the substitution of E101D. The electron density map for D101 of LISA-314 was improved after the introduction of shorter aspartate residue and the reduction of flexibility compared to E101 of SA-WT (Fig. 1-3D). Interestingly, the space group of the crystal of LISA-314 changed to *C*2 from the $P2_1$ of the SA-WT, even though both crystals were obtained using the same crystallization conditions. This difference in the crystal packing was rationalized below.

The conformational changes were mainly caused by the substitutions of Y22S and R103K (Fig. 1-3A, E), but the *B* factors were not affected (Fig. 1-4). One change is the flip of the C-terminal loop (residues 133–134) owing to the substitution of Y22S. The disappearance of the CH/π interaction between Y22 and K134 near the C-terminus is thought to be the reason for the flip as it is sometimes observed in the SA structures deposited in the Protein Data Bank. The second is the change in the hydrogen bond network resulting from the substitution of R103K. The hydrogen bond between R103 and T129, which was formed in 2/4 chains of SA-WT, was changed to that between K103 and T131 (a new hydrogen bond partner) as a result of the substitution. The last substitution site at E116N did

not change the *B* factor, although the electron density for the side chain of N116 was clearly obtained (Fig. 1-3F). Other than these substitution sites, decreased *B* factors were observed at residue numbers 32–35. The crystal packing was changed from *C*2 to $P2_1$ owing to the substitution of Y22S, and this region interacted with a neighboring molecule in the new crystal form, which may be the reason for the decrease in *B* factors.

Generally, the higher the *B* factor value, the more flexible the corresponding region in the protein, and vice versa. This attribute has been used to predict linear B-cell epitopes (*76*). However, any large conformational changes corresponding to the large reduction of *B* factors around the substituted sites were not observed. Even higher *B* factors were measured because of the substitutions. The effect of substitutions is restricted mainly to the changes of side chains at the substituted sites. From these results, if the lowered immunogenicity of LISA-314 is caused by the conformational changes, it is presumed that it is not caused by the conformational change of the whole structure, but by the local conformational changes at the substituted sites.

In this study, the author have proven that LISA-314 has both low immunogenicity and high biotin-binding affinity without a striking change in the whole structure, despite introducing six amino-acid substitutions. Practically, the author expects LISA-314 to be useful in pre-targeting cancer therapy. However, as mentioned in General Introduction, some clinical studies showed that the endogenous BTN can effectively block the BTN-binding pocket of administrated SA, impairing the efficiency of the pre-targeting method (*57, 58*). To solve this problem, the binding site of LISA-314 has to be modified to selectively bind to the non-natural BTN analog without interference of endogenous BTN. This detailed structural information will be useful for improvement of LISA-314.

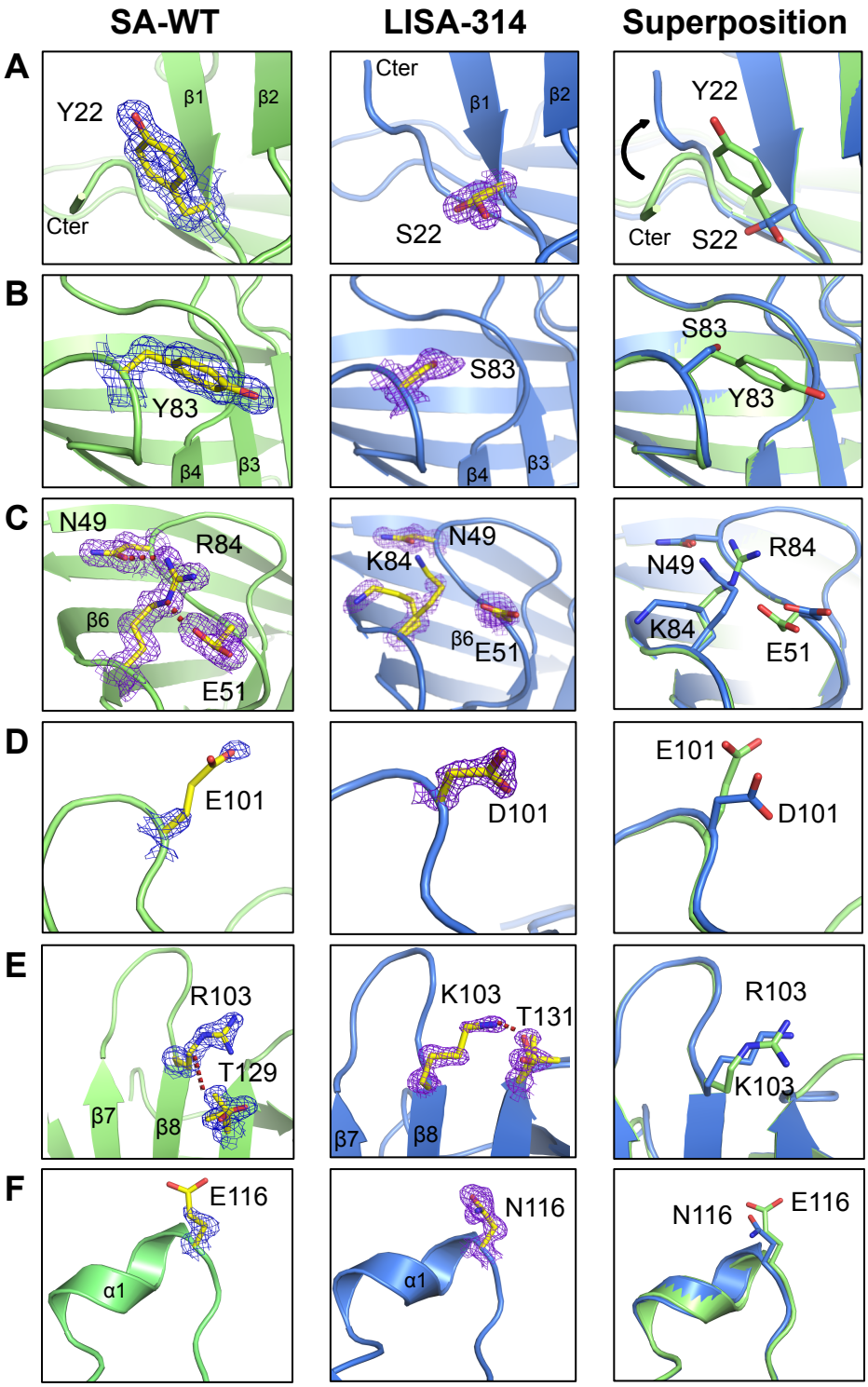

Fig. 1-3. Structural change of SA induced by six amino-acid substitutions.
The electron density maps of SA-WT (green) and LISA-314 (blue) are shown in the first and the second lanes, respectively (blue mesh; the 2*Fo*–*Fc* electron density map contoured at 1.0 σ). Superimposed structures between SA-WT and LISA-314 are shown in the third lane. The panels are displayed around (A) Y22S, (B) Y83S, (C) R84K, (D) E101D, (E) R103K, and (F) E116N, respectively.

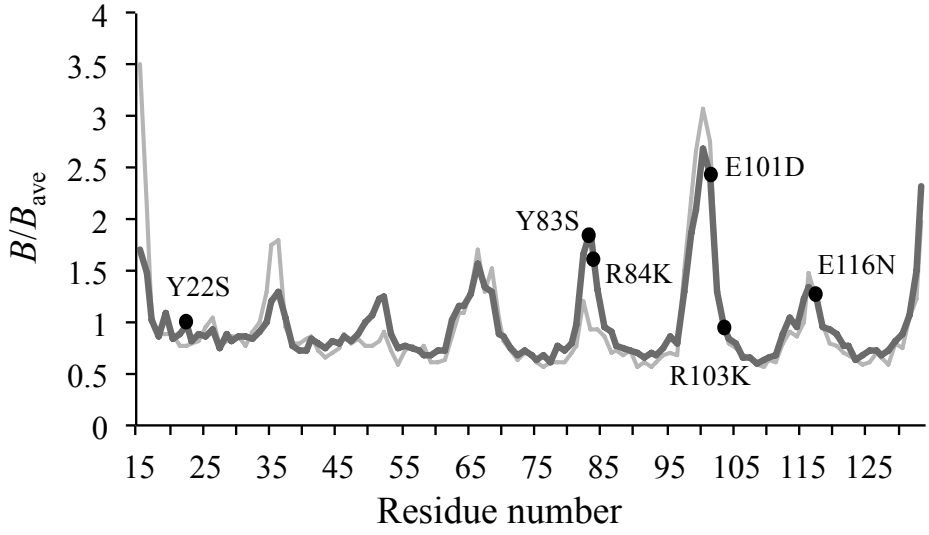

Fig. 1-4. Comparison of relative temperature (*B*) factors between SA-WT (thin line) and LISA-314 (thick line). The *B* factor for Cα atom of each amino acid is standardized by the equation: *B* factor/B_{ave} (B_{ave}: the average *B* factor of the whole Cα atoms).

1.4. Summary

Here, the author performed high-resolution X-ray structural analyses of LISA-314 and SA-WT to investigate the effect of substitutions on the three-dimensional structure and the correlation between decreased immunogenicity and the structure. LISA-314 forms a tetramer in the same manner as wild-type streptavidin. The binding mode of BTN in LISA-314 is also completely identical to that in wild-type streptavidin, and conformational changes were observed mostly at the side chains of substituted sites. Any large conformational changes corresponding to the reduction of *B* factors around the substituted sites were not observed. These results demonstrated the LISA-314 acquired low immunogenicity without losing structural properties of SA-WT.

Chapter 2

Structure-based design of a streptavidin mutant high specific for an artificial biotin analog

2.1. Introduction

In chapter 1, it was revealed that LISA-314 improved immunogenicity while it well retained the structure of wild-type SA-WT. However, for the application to pre-targeting method, the second problem regarding endogenous BTN species must be solved. They bind to LISA-314 strongly and interfere the binding of the exogenous radiolabeled BTN derivative (*57, 58*).

Here, the author presents a modified LISA-314 that binds to a newly designed artificial BTN analog, and has no binding affinity for a natural BTN species, biocytin. This is the first SA binding system without any influence from endogenous BTN species.

2.2. Materials and Methods

2.2.1. Expression and purification of V21 mutant

The nucleotide sequence of the V21 mutant, which contains amino-acid substitutions Y22S/Y83S/R84K/E101D/R103K/E116N/N23D/S27D, was subcloned into the pCold TF vector (Takara Bio). The HRV 3C protease cleavage site, the coding sequence of Trigger Factor (TF) and the 6×His tag were fused at the N-terminus of V21. *Escherichia coli* BL21Star(DE3) cells harboring the V21 plasmid were grown at 37 °C in Luria Broth containing 100 μg/ml ampicillin up to an OD of 0.5–0.6, induced with isopropyl-β-D-thiogalactopyranoside (IPTG) to a final concentration of 0.4 mM and further grown at 15 °C for 24 h. Cells were harvested by centrifugation at 8000 × *g* for 20 min

and resuspended in a lysis buffer containing 1× PBS, 500 mM NaCl, 20 mM imidazole, cOmplete EDTA-free protease inhibitor cocktail tablets (Roche) and Benzonase (Novagen). The sample was lysed by passing through an EmulsiFlex (AVESTIN) and centrifuged at 10,000 × *g* for 30 min. The supernatant was loaded onto Ni agarose (Invitrogen) and washed with the lysis buffer. V21 was eluted from the column with elution buffer (1× PBS and 250 mM imidazole). HRV 3C protease was added to the sample at 1:50 molar ratio. After incubation at 4 °C for 2 d, the solution was dialyzed against buffer (1× PBS, 500 mM NaCl and 20 mM imidazole) and loaded onto a HisTrap HP column (Invitrogen) to remove His-tagged material. The flow-through was collected and reloaded onto the column. The flow-through was then recollected and dialyzed against buffer (25 mM Tris-HCl, 500 mM NaCl and 4 M GdnHCl). The dialysate was then passed through a HisTrap HP column. The flow-through was collected and dialyzed against buffer (10 mM Tris-HCl, pH 7.5 and 250 mM NaCl). Ligand (BTN, BTNtail, or IMNtail) was added to the V21 sample at a 20:1 molar ratio. The proteins were then concentrated to approximately 10 mg/ml, as estimated by absorbance at 280 nm.

2.2.2. Expression and purification of S45-substituted mutants of V21

The nucleotide sequences of S45-substituted mutants (S45T, S45N, S45Q, S45H, S45L, S45I, S45A; V212 is the S45N mutant) of V21 were subcloned into the pET21a(+) vector (Novagen). For preparation of the muteins, the isolation and refolding protocols were performed as described in previous reports (*77-80*) with modifications. The T7 tag was introduced at the N-terminus of the muteins and a 6×His tag at the C-terminus. BL21Star(DE3) cells harboring the mutant plasmid were grown at 37 °C in 2×YT medium containing 100 μg/ml ampicillin to an OD of 0.8, and protein expression induced by adding IPTG to a final concentration of 1 mM and cells grown at 37 °C for a further 5 h. Cells were harvested by centrifugation at 8000 × *g* for 20 min and resuspended in a lysis

buffer containing 50 mM Tris-HCl, pH 8.0, and ruptured by sonication. The lysed cells were centrifuged at 16,500 × *g* for 20 min. The insoluble fraction was washed three times with buffer (50 mM Tris-HCl, pH 8.0 and 2% Triton X-100) and then washed twice with ultra-pure water. The inclusion bodies were dissolved in 6 M guanidine hydrochloride, pH 1.5, and dialyzed against the dissolution buffer at 4 °C overnight. Insoluble material was removed by ultracentrifugation at 16,500 × *g* and 4 °C for 30 min, and the supernatant was added to the refolding buffer (50 mM Tris-HCl, pH 8.0, 400 mM L-arginine hydrochloride, 200 mM NaCl and 1 mM EDTA) by the rapid refolding method and left for 2 d. The sample was loaded onto Complete His-tag Purification resin (Roche) and eluted with a refolding buffer containing 400 mM imidazole. The eluted sample was buffer-exchanged into gel-filtration buffer (1×PBS) by dialysis. Further purification was carried out by gel-filtration chromatography using a HiLoad 16/600 Superdex 75 column. IMNtail was added to the sample at an 8:1 molar ratio. Finally, the purified protein was buffer-exchanged and concentrated to 10 mg/ml in 20 mM Tris-HCl buffer (pH 7.5) containing 200 mM NaCl using Vivaspin 10-kDa cutoff (GE Healthcare). BTNtail and IMNtail are gifts from co-workers (*81*). In the case of using the refolding buffer without L-arginine hydrochloride, samples were aggregated.

2.2.3. Binding assays by SPR

SPR measurements were performed by co-worker (*81*).

2.2.4. Crystallization

Crystallization was performed by the sitting-drop vapor-diffusion method at 20 °C in Violamo 96-well plates (As One, Osaka, Japan). Sixty microliters of the reservoir solution was added to each well of the 96-well plates. Crystals of V21 complexed with BTN were obtained by mixing 0.5 μl of

the protein solution and 0.5 µl of the reservoir solution (100 mM sodium acetate trihydrate, pH 4.6 and 2 M ammonium sulfate). Crystals of V21 complexed with BTNtail were grown by mixing 0.1 µl of the protein solution with 0.1 µl of the reservoir solution (0.1 M cadmium chloride hydrate, 0.1 M sodium acetate trihydrate, pH 4.6 and 30% (w/v) PEG400). Crystals of V21 complexed with IMNtail were prepared by mixing 0.5 µl of the protein solution and 0.5 µl of the reservoir solution (0.2 M sodium citrate tribasic dehydrate, 0.1 M HEPES sodium, pH 7.5 and 35% w/v (+/-)-2-methyl-2, 4-pentandiol). Crystals of V212 complexed with IMNtail were obtained by mixing 0.5 µl of the protein solution and 0.5 µl of the reservoir solution (60 mM sodium cacodylate trihydrate, pH 6.8 and 27% (w/v) PEG300).

2.2.5. X-ray data collection and structure determination

The dataset for V21 complexed with BTNtail were collected on the beamline BL17A at the Photon Factory (Tsukuba, Japan), and all the other datasets were collected on the BL44XU at SPring-8 (Harima, Japan) at −173 °C. A crystal of V21 complexed with BTNtail was cryoprotected by coating with a solution (66.5% Paratone-N, 28.5% Paraffin Oil and 5% Glycerol). Crystals of V21 complexed with BTN and IMNtail and V212 complexed with IMNtail were cryoprotected by the well solution containing 20% (v/v) glycerol. Data were indexed and scaled with the programs *DENZO* and *SCALEPACK* from the *HKL2000* program suite (HKL Research). The structures were solved by molecular replacement with the program *Phaser (64)* from the *CCP4i* package (*65*) using the crystal structure of LISA-314 (PDB ID: 3WYQ, unreleased data (*82*)) as the search model. The resultant structures were manually modified to fit into the experimental electron density maps, using the program *Coot (66)*, then refined with the program *Refmac5* (*67*) from the *CCP4i* package. The results of the structural analysis are summarized in Table 2-1. Figures were prepared with *Pymol*

(http://www.pymol.org/). The final structure coordinates and structure factor amplitudes were deposited into the Protein Data Bank with IDs 3WZN for V21 complexed with BTN, 3WZO for V21 complexed with BTNtail, 3WZP for V21 complexed with IMNtail, and 3WZQ for V212 complexed with IMNtail.

Table 2-1. Data collection and refinement statistics.

	V21-BTN	V21-BTNtail	V21-IMNtail	V212-IMNtail
Data collection				
Space group	$P2_12_12$	$P2_12_12_1$	$P2_1$	$C222_1$
Unit-cell parameters (Å, °)	a = 67.68	a = 55.24	a = 59.97	a = 77.42
	b = 54.34	b = 85.46	b = 57.50	b = 77.41
	c = 60.06	c = 86.12	c = 71.18	c = 172.80
			β = 103.34	
Wavelength	0.98000	0.98000	0.90000	0.90000
Resolution (Å)	50–1.30 (1.35–1.30)[a]	50–1.50 (1.55–1.50)	50–1.20 (1.24–1.20)	50–1.70 (1.76–1.70)
R_{sym} (%)[b]	7.2 (40.6)	3.5 (23.2)	6.8 (30.9)	5.4 (35.3)
Total reflections	411,780	405,051	497,753	326,970
Unique reflections	54,829 (5,393)	64,021 (6,294)	143,314 (13,724)	55,926 (5,415)
$I/\sigma(I)$	26.8 (4.0)	17.6 (3.1)	18.3 (2.8)	26.4 (3.0)
Completeness (%)	99.1 (99.2)	97.4 (97.2)	96.6 (93.0)	97.0 (94.8)
Redundancy	7.5 (5.5)	6.3 (4.4)	3.5 (2.6)	5.8 (3.6)
Refinement				
Resolution	1.30	1.50	1.20	1.70
No. of reflections	51,662	60,475	135,778	52,687
R_{work} (%)[c]/R_{free} (%)[d]	16.0/20.1	17.3/23.6	13.4/16.1	19.7/24.4
No. of atoms				
Protein	1,840	3,734	3,656	3,713
Ligand/ion	37	159	126	128
Water	222	233	441	287
B factors				
Protein	14.8	14.7	10.0	18.6
Ligand/ion	14.6	33.6	14.4	35.2
Water	29.8	34.7	24.9	29.0
R.m.s deviations				
Bond length (Å)	0.026	0.018	0.026	0.025
Bond angles (°)	2.33	1.91	2.27	2.12
Ramachandran plot				
Favored (%)	96.15	95.39	97.01	94.56
Allowed (%)	3.42	3.56	2.99	5.44
Outliers (%)	0.43	1.05	0.00	0.00
PDB IDs	3WZN	3WZO	3WZP	3WZQ

[a]Values in parentheses are for the highest-resolution shell.

[b]R_{sym} is calculated as $\Sigma_{hkl}\Sigma_i|I_i(\text{hkl}) - \langle I(hkl)\rangle|/\Sigma_{hkl}\Sigma_i I(hkl)$, where $I_i(hkl)$ is the intensity of an individual measurement of the reflection with Miller indices *hkl* and $\langle I(hkl)\rangle$ is the average intensity from multiple observations.

[c]$R_{work} = \Sigma_{hkl}||F_{obs}| - |F_{calc}||/\Sigma_{hkl}|F_{obs}|$, where F_{obs} and F_{calc} are the observed and calculated structure-factor amplitudes, respectively.

[d]R_{free} is computed in the same manner as R_{work} but using only a small set (5%) of randomly chosen intensities that were not used in the refinement of the model.

2.3. Results and Discussion

2.3.1. Construction of V21 from the original LISA-314

To develop a pre-targeting method using the SA binding system, it is essential to solve the problem that BTN present as a vitamin in the body strongly binds to LISA-314. Thus, a novel binding system is required, in which the original LISA-314 selectively binds to a non-natural BTN analog without binding endogenous BTN species. The author may therefore consider two strategies: the modification of LISA-314 and the development of a new, non-natural BTN analog.

Reznik *et al.* (*59*) prepared a double mutant of N23A/S27D that acquired a higher binding affinity for IMN than BTN with K_d values of 1.0×10^{-6} M and 7.1×10^{-5} M, respectively (*59*). Considering the report, a double substitution N23D/S27D was introduced into LISA-314 (naming the resulting mutant "V21"). The reason why N23D was adopted instead of N23A is as follows. The author presumed that N23D would induce electrostatic repulsion against the ureido oxygen of BTN and make the affinity lower for BTN than N23A, because the ureido oxygen is highly polarized in positive (*83*). Besides, negatively charged aspartate residue would interact with the guanidino nitrogen of IMN, which is protonated at neutral pH (*84*). Although more electrostatic repulsion against the ureido oxygen of BTN was introduced in V21 (Fig. 2-1A), a lower K_d value of 1.0×10^{-7} M for BTN (cf. 7.1×10^{-5} M from Reznik *et al.*) and that of 3.5×10^{-7} M for biocytin was measured by surface plasmon resonance (SPR) (see below). The author is now crystallizing the N23A/S27D mutant to elucidate structural basis explaining the affinity difference from V21.

2.3.2. Crystal structure of V21 in complex with BTN

The crystal structure of V21 in complex with BTN was solved at 1.3 Å resolution. The structure forms a tetramer, which is composed of a dimer of dimers. One BTN molecule binds to each

protomer. No major conformational changes occurred in the overall structure when compared with LISA-314.

A comparison between the binding motif of BTN in V21 and that in LISA-314 showed that three residues 23, 27 and 128 interacted differently with BTN (Fig. 2-1). The distance between the carboxyl oxygen of Asp23 in V21 and the ureido oxygen of BTN is 4.47 Å. The carboxyl oxygen of Asp27 forms van der Waals contact but not hydrogen bond with the ureido oxygen because of the improper orientation despite the relatively short distance between them (i.e., 3.19 Å and 3.29 Å, Fig. 2-1C, D), showing that two hydrogen bonds around the ureido oxygen in LISA-314 were lost in V21. As a result, the position of the ureido oxygen of BTN in V21 moved away from Asp23 and Asp27 by 0.68 Å relative to that in LISA-314. Moreover, the interaction between the carboxyl oxygen of Asp128 and the N^3 nitrogen of BTN was altered from a direct hydrogen bond in the LISA-314-BTN complex to interaction *via* a water molecule in the V21-BTN complex.

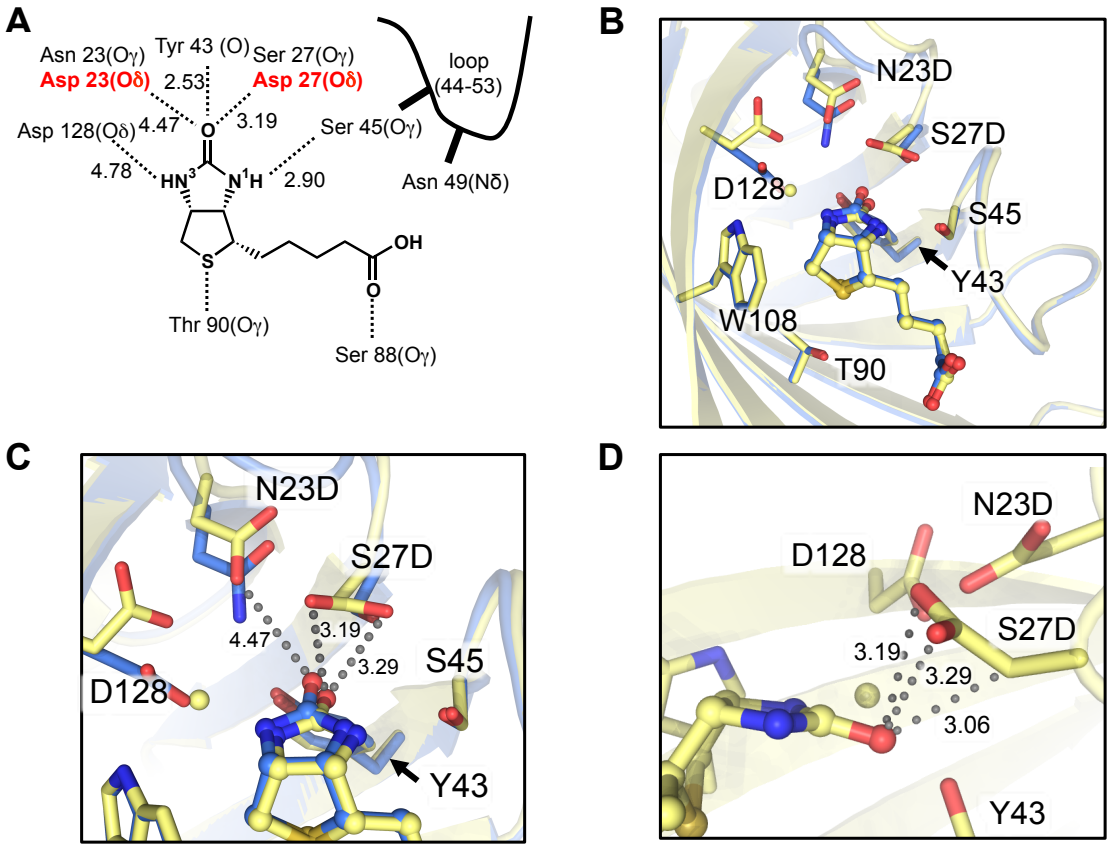

Fig. 2-1. Binding mode of BTN in V21. (A) The distance between BTN and V21 are shown by the black dotted lines. The position numbers of nitrogen atoms are shown as superscripts. Residues in LISA-314 are indicated in black and substituted residues in V21 are in red. The distances (Å) between residues of V21 and BTN are represented schematically. (B) Superposition of the BTN bound to V21 (yellow) was performed with the BTN bound to LISA-314 (PDB ID: 3WYQ: blue). (C) A close-up view around N23D/S27D residues in (B). The distance (Å) between BTN and residues in V21 is also shown (gray dot lines). (D) The structure around BTN and S27D in V21 is shown.

From the structural analysis results of V21, the author concludes that N23D/S27D substitutions induce electrostatic repulsions against the ureido oxygen atom, breaking two main hydrogen bonds with BTN. Although the binding affinity of V21 for BTN was lower than that of the N23A/S27D mutant in Reznik *et al*. (*59*), no structural change was seen in the overall structure.

2.3.3. Design and synthesis of BTN analogs, BTNtail and IMNtail

Next, non-natural BTN derivatives were designed as new ligand molecules for SA. It was predicted that addition of a long spacer between BTN and a drug molecule was needed for future pre-targeting therapy. One study reported that the carboxyl terminus of BTN was modified for extension (*85*), and thereby a BTN molecule with a long tail (BTNtail) was designed (Fig. 2-2A). A structural analysis of BTNtail-bound V21 at 1.5 Å resolution (Fig. 2-2B) demonstrated that the binding motif of BTNtail in V21 is very similar to that of BTN; although, the sulfur atom of the BTNtail was oxidized by unknown reason as observed in previous reports (*74, 75*). In summary, the addition of the long tail had no influence on the binding mode of BTNtail in V21 when compared with the binding mode of BTN.

The author also examined the addition of a long tail to IMN (IMNtail) as a new ligand and this ligand was synthesized (Fig. 2-3A). SPR measurements showed that V21 had a K_d value of 1.5×10^{-7} M for IMNtail at neutral pH (see below). Conversely, LISA-314 showed no binding affinity towards the IMNtail, which is interesting because SA-WT possessing an identical BTN binding motif to LISA-314 is known to have significant binding affinity toward IMN ($K_d = 1.3 \times 10^{-7}$ M at neutral pH) (*59*). The tail region of IMNtail might have dramatically lowered its binding ability to LISA-314.

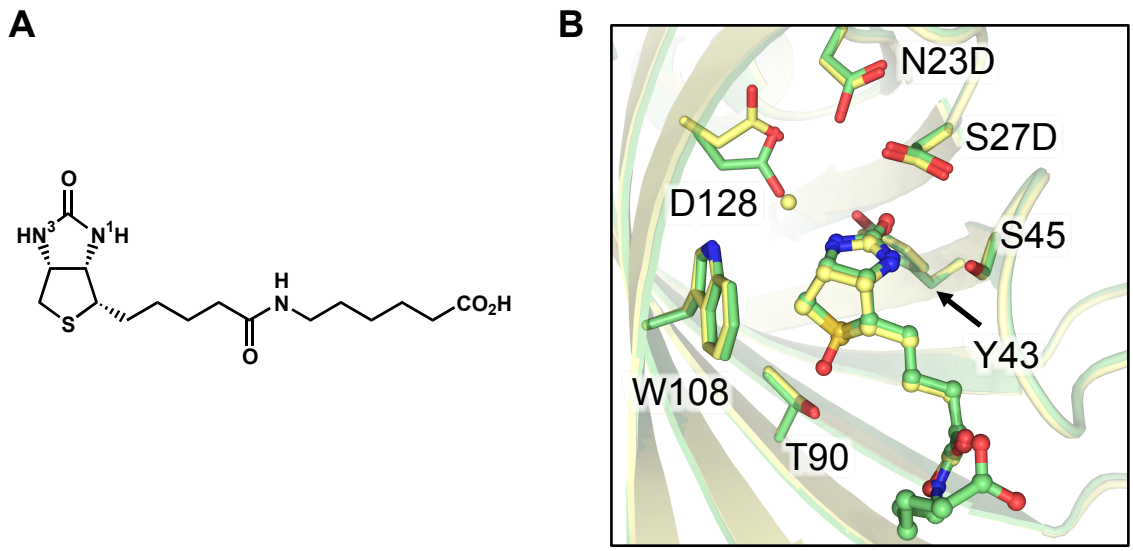

Fig. 2-2. Binding mode of BTNtail in V21. (A) Structural formula of BTNtail. (B) Structural superposition of BTNtail-bound V21 (green) with the BTN-bound V21 (yellow).

2.3.4. Crystal structure of V21 in complex with the IMNtail

The crystal structure of V21 in complex with IMNtail was determined at 1.2 Å resolution. One IMNtail molecule binds to each protomer (Fig. 2-3B). Superposition of the complex structures between V21-IMNtail and V21-BTNtail shows that a head group of IMNtail shifts toward Asp128 compared to that of BTNtail (Fig. 2-3C). Besides, the N^2 nitrogen of IMNtail interacts with Asp27, with which the ureido oxygen of BTN has no interaction in V21 because of electrostatic repulsion (Fig. 2-3D). The shift of the head group to Asp128 causes a rearrangement of the hydrogen-bond network. The distances between the N^2 nitrogen of IMNtail and the carboxyl oxygen of Asp23 or the hydroxyl oxygen of Tyr43 are lengthened to 3.61 and 3.50 Å, respectively, indicating a weaker contribution to hydrogen bonding by Asp23 and Tyr43 than that observed in SA-WT (3.2 and 2.7 Å, respectively) (*84*). The S27D substitution, which gives a longer side chain, may push the N^2 nitrogen of IMNtail away from Asp23 and Tyr43 and towards Asp128.

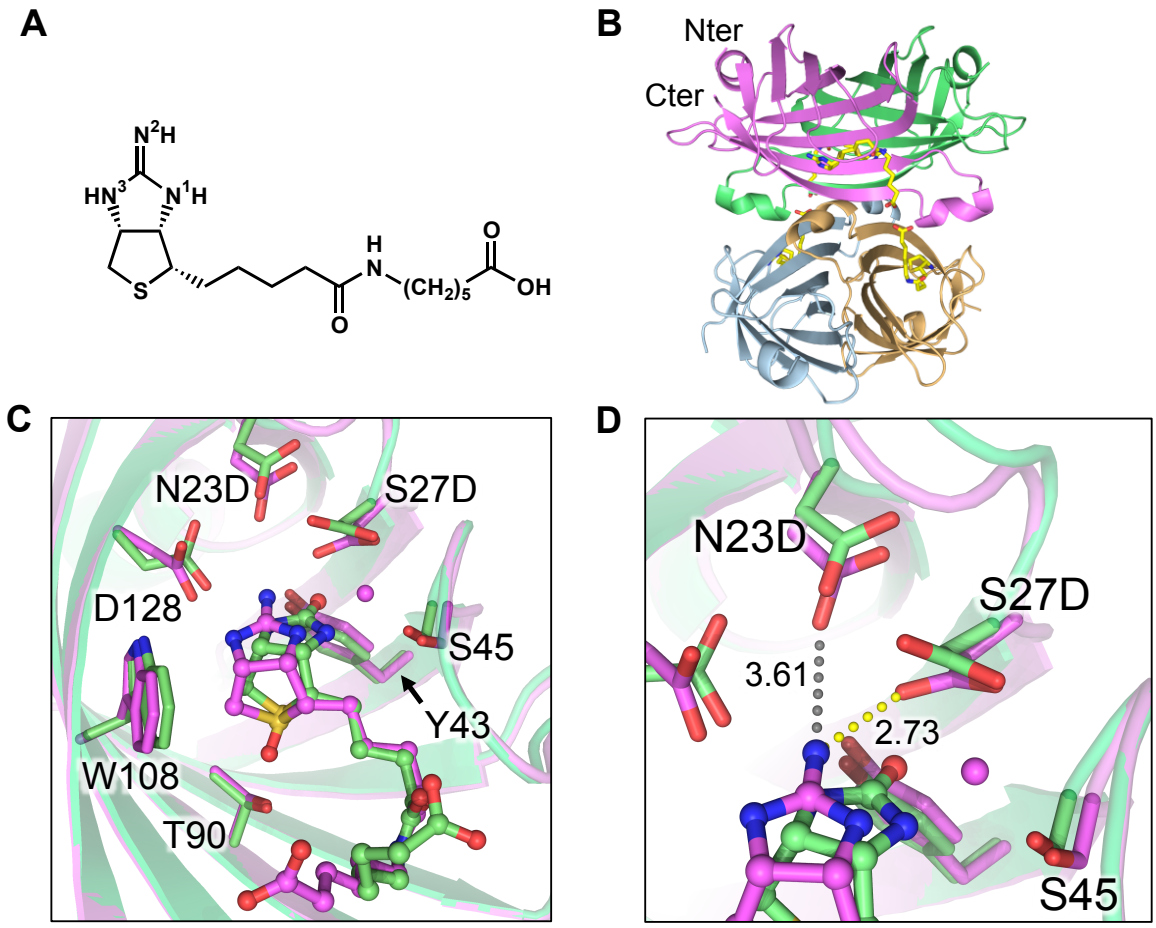

Fig. 2-3. Binding mode of IMNtail in V21. (A) Structural formula of IMNtail. The position numbers of nitrogen atoms are shown in superscripts. (B) Structure of V21 tetramer (ribbon model) in complex with IMNtail (stick model). (C) Superposition of BTNtail-bound V21 (green) and IMNtail-bound V21 (magenta) structures. (D) A close-up view around N23D/S27D residues in (C). Numbers indicate the distance (Å) between IMNtail and residues in V21 (gray dot line: non hydrogen bond, yellow dot line: hydrogen bond).

Interestingly, the most striking difference between the structures of V21-BTNtail and V21-IMNtail complexes was found at the hydrogen bond with Ser45 (Fig. 2-4). Although Ser45 directly forms a hydrogen bond to N^1 nitrogen of BTNtail in V21 (2.96 Å, Fig. 2-4A), as it does in SA-WT (2.90 Å), it indirectly forms a hydrogen bond to N^1 nitrogen of IMNtail *via* a water molecule (Ser45-N^1 distance: 4.39 Å, Fig. 2-4B). Because of this difference, the author proposed that a substitution at Ser45 in V21 to a residue with a bulky side chain would eliminate the binding affinity for BTNtail through steric hindrance without affecting the binding of IMNtail. The author made a

single amino-acid substitution from serine to threonine, asparagine, glutamine, histidine, leucine, or isoleucine, with alanine as a negative control.

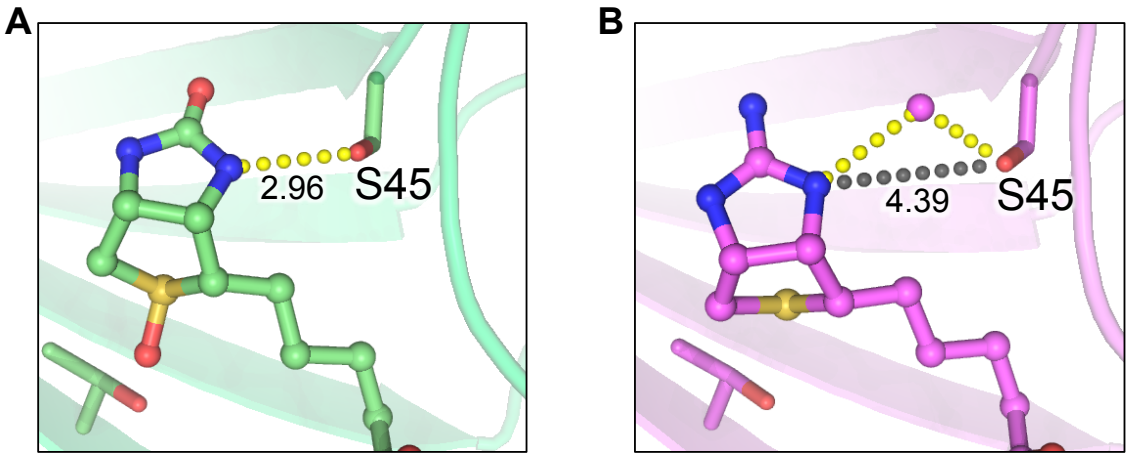

Fig. 2-4. Interactions between Ser45 and ligands. The interaction (A) between Ser45 and BTNtail (B) between Ser45 and IMNtail is shown. Hydrogen bonds are shown as yellow dot lines. Numbers indicate the distance (Å) (gray dot line: non hydrogen bond, yellow dot line: hydrogen bond).

2.3.5. Evaluation of the amino-acid substitutions at Ser45 of V21

Out of the seven substitution mutants of V21, only S45L and S45I mutants could not be expressed in *E. coli*. The binding affinities of the V21 mutants for ligands were measured by SPR (Table 2-2). The S45A and S45T mutants had significantly decreased affinities for biocytin by 10–100-fold compared with V21, while maintaining binding affinities for IMNtail. As expected, the S45N, S45Q and S45H mutants, with more bulky residues, completely lost binding affinity for biocytin. Among these, S45N and S45H mutants retained binding affinity of about the order of 10^7 for the non-natural IMNtail, which is similar to the original V21. Since the isoelectric point of histidine residue is near neutral pH and S45H mutant might show unstable binding property in wider pH range, the S45N mutant, termed V212, was examined in the subsequent development.

Table 2-2. SA muteins, substituted residues and results of SPR measurements

Muteins	Substituted residues	K_d (M)	
		Biocytin	IMNtail
LISA-314		8.3×10^{-11}	not detected
V21	N23D, S27D	3.5×10^{-7} (1.0×10^{-7} [a])	1.5×10^{-7}
V212	N23D, S27D, S45N	not detected	5.9×10^{-7}
	N23D, S27D, S45H	not detected	5.2×10^{-7}
	N23D, S27D, S45Q	not detected	not detected
	N23D, S27D, S45A	2.4×10^{-5}	3.2×10^{-7}
	N23D, S27D, S45T	7.6×10^{-6}	7.6×10^{-7}

[a] The K_d value was measured with biotin.

2.3.6. Crystal structure of V212 in complex with IMNtail

To investigate the effect of the S45N substitution, the crystal structure of V212 in complex with IMNtail was solved at 1.7 Å resolution. V212 also forms a tetramer and one IMNtail molecule binds to each protomer. A comparison of the binding pocket of the V212-IMNtail complex to that of the V21-IMNtail complex showed that the binding loop composed of residues 45–52 in V212 was formed differently to the same loop in V21 (Fig. 2-5A). The binding loop in V212 does not interact with the IMNtail molecule. When a ligand binds, the binding loop usually changes from a flexible open conformation to a close conformation like a lid over the binding pocket (*68, 70, 86*). Even in the complex with IMNtail, the binding loop in V212 showed an open conformation as well as in the ligand-free SA-WT (Fig. 2-5B). Although the electron densities are not well ordered, the side chain of Asn45 in V212 appears to interact with Gly48, Asn49 and Ser52 to maintain the opened loop conformation (Fig. 2-5A, C). This is similar to the characteristic interaction between Ser45 and Ser52 found in the ligand-free SA-WT to stabilize the opened loop (*68, 70, 86*).

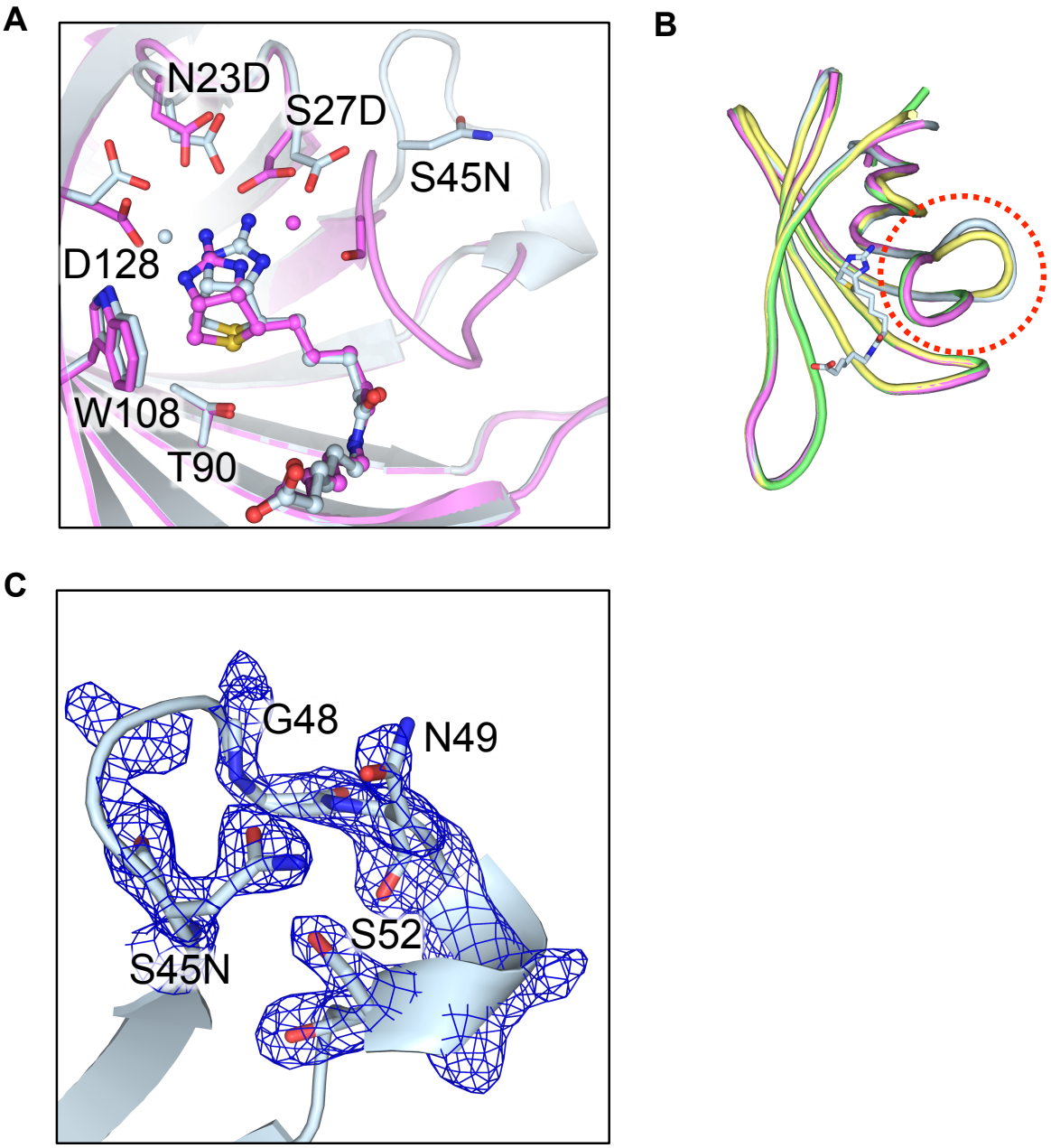

Fig. 2-5. Binding mode of IMNtail in V212. (A) Superposition of IMNtail-bound V212 (cyan) and IMNtail-bound V21 (magenta) structures. (B) Structural superposition of the V212-IMNtail protomer (cyan) with the V21-IMNtail (magenta), SA-WT-BTN (green) and SA-WT-apo (yellow) protomers. For clarification, the ligand is only depicted for IMNtail bound in V212 as a stick model. The loop composed of residues 45–52 is indicated with a circle of red dots. (C) The 2*Fo*–*Fc* electron density map around residues of N45-S52 of the V212-IMNtail complex is shown (blue mesh: contoured at 1.0 σ).

The author infers that the S45N substitution sterically hinders the head group of IMNtail, so the ligands and Asn45 are unable to make interactions. Thus, the Asn45 flips away from IMNtail to force the binding loop to adopt the open conformation. An initial expectation was that this steric hindrance effect by introducing the S45N substitution occurred only for BTNtail based on the distance between Ser45 and the N^1 nitrogen of BTNtail or IMNtail in V21, but it seems to occur also for IMNtail to some extent.

However, interestingly, the K_d values of IMNtail are comparable between V21 and V212 (Table 2-2) despite the structural change of the binding loop from the closed form found in V21 to the open form observed for V212, resulting in loss of interactions between the binding loop and IMNtail (Fig. 2-5, 2-6). The interaction of Ser45 with the N^1 nitrogen of IMNtail *via* a water molecule observed in V21 was lost in V212. Instead, Asp27 forms a hydrogen bond with the N^1 nitrogen of IMNtail through a water molecule in V212. In addition, the hydrogen bond distances between the carboxyl oxygen of Asp23 and the N^2 nitrogen of IMNtail was 3.61 Å for V21 and 2.75 Å for V212, indicating that the weak hydrogen bond in V21 was strengthened in V212 (Fig. 2-6).

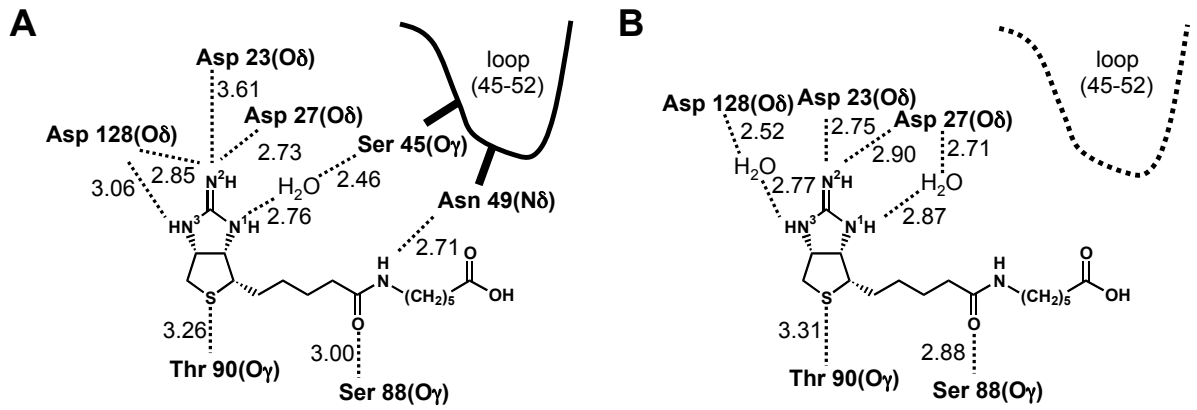

Fig. 2-6. Schematic representations of the interactions between IMNtail and (A) V21 or (B) V212. The position numbers of nitrogen atoms are shown in superscripts. The loop in V212 is presented with the dash-dot lines, because it forms an open conformation and does not interact with the ligand. The distances (Å) between amino-acid residues and IMNtail are represented by dotted lines.

The author postulates that these unique interactions in V212 may compensate for the loss of the interaction between the binding loop and IMNtail and maintain affinity for IMNtail comparable to V21. In contrast to the IMNtail, the BTN and BTNtail molecules cannot form a hydrogen bond with Asp23 or Asp27 because of electrostatic repulsion as described above, and they would suffer severe steric hindrance by the S45N substitution. The author concludes these differences decide the outcome; V212 abolishing affinity only for BTN species. the present study, we have created a novel SA binding system, V212 and IMNtail, by modifying the low immunogenic mutant LISA-314. While abolishing the binding affinity for a BTN species, biocytin, V212 can bind the non-natural BTN analogue, IMNtail, with a K_d value of 5.9×10^{-7} M. This promises that V212 can capture the IMNtail in the human body without any binding competition from endogenous BTN species. This is the first SA binding system without any influence from endogenous BTN species.

2.4. Summary

In this chapter, the author improved the binding pocket of LISA-314 to abolish its binding affinity for endogenous biotin species and establish a strong affinity binding for artificial biotin analog. The replacement of three amino acid residues was performed in two steps to develop a mutant termed V212, which selectively binds to IMNtail. SPR measurements showed that V212 has a K_d value of 5.9×10^{-7} M towards IMNtail, while binding affinity for endogenous biotin species was not detected.

Chapter 3

Structure-based design of a bivalent iminobiotin analog showing strong affinity toward a low immunogenic streptavidin mutant

3.1. Introduction

In chapter 2, the modified LISA-314 binding system without any influence from endogenous BTN species was developed, namely V212/IMNtail system. However, the binding affinity of V212 for IMNtail was relatively low compared with the original binding affinity of SA/BTN. Thus, further modifications are necessary before it can be used practically in a pre-targeting system.

This chapter describes the development of a new ligand that binds to V212 with much higher affinity compared to IMNtail.

3.2. Materials and methods

3.2.1. Expression and purification of V212 mutant

The nucleotide sequence of V212 was subcloned into the pET21a(+) vector (Novagen). For preparation of the muteins, the isolation and refolding protocols were performed as described in previous reports (*77-80*) with modifications. The T7 tag was introduced at the N-terminus of the muteins and a 6×His tag at the C-terminus. BL21Star(DE3) cells harboring the mutant plasmid were grown at 37 °C in 2×YT medium containing 100 μg/ml ampicillin to an OD of 0.8, and protein expression induced by adding IPTG to a final concentration of 1 mM and cells grown at 37 °C for a

further 5 h. Cells were harvested by centrifugation at 8000 × *g* for 20 min and resuspended in a lysis buffer containing 50 mM Tris-HCl, pH 8.0, and ruptured by sonication. The lysed cells were centrifuged at 16,500 × *g* for 20 min. The insoluble fraction was washed three times with buffer (50 mM Tris-HCl, pH 8.0 and 2% Triton X-100) and then washed twice with ultra-pure water. The inclusion bodies were dissolved in 6 M guanidine hydrochloride, pH 1.5, and dialyzed against the dissolution buffer at 4 °C overnight. Insoluble material was removed by ultracentrifugation at 16,500 × *g* and 4 °C for 30 min, and the supernatant was added to the refolding buffer (50 mM Tris-HCl, pH 8.0, 400 mM L-arginine hydrochloride, 200 mM NaCl and 1 mM EDTA) by the rapid refolding method and left for 2 d. The sample was loaded onto Complete His-tag Purification resin (Roche) and eluted with a refolding buffer containing 400 mM imidazole. The eluted sample was buffer-exchanged into gel-filtration buffer (1×PBS) by dialysis. Further purification was carried out by gel-filtration chromatography using a HiLoad 16/600 Superdex 75 column. Bis-IMNtail was added to the sample at an 8:1 molar ratio. Finally, the purified protein was buffer-exchanged and concentrated to 10 mg/ml in 20 mM Tris-HCl buffer (pH 7.5) containing 200 mM NaCl using Vivaspin 10-kDa cutoff (GE Healthcare). Bis-IMNtail is a gift from co-workers (*87*).

3.2.3. Binding assays by SPR

SPR measurement was performed by co-worker (*87*).

3.2.4. Crystallization

Crystallization was performed by the sitting-drop vapor-diffusion method at 20 °C in Violamo 96-well plates (As One, Osaka, Japan). Sixty microliters of the reservoir solution was added to each well of the 96-well plates. Crystals were obtained by mixing 0.1 μL of protein solution (10 mg/mL

Bis-IMNtail-bound V212, 20 mM Tris-HCl, pH 7.5 and 200 mM NaCl) and 0.1 μL of reservoir solution (0.2 M sodium fluoride and 20% PEG3350).

3.2.5. X-ray data collection and structure determination

All datasets were collected on the beamline at BL44XU at SPring-8 (Harima, Japan) under −173 °C. A crystal of V212 complexed with Bis-IMNtail was cryoprotected by a well solution containing 20% glycerol. Data were indexed and scaled with the programs *DENZO* and *SCALEPACK* from the *HKL2000* program suite (HKL Research). The structure was solved by molecular replacement with the program *Phaser (64)* from the *CCP4i* package (*65*) using the crystal structure of LISA-314 (PDB ID: 3WYQ, unreleased data (*82*)) as the search model. The resultant structure was manually modified to fit into the experimental electron density maps, using the program *Coot (66)*, then refined with the program *Refmac5* (*67*) from the *CCP4i* package. The results of the structural analysis are summarized in Table 3-1. Figures were prepared with *Pymol* (http://www.pymol.org/*)*. The final structure coordinates and structure factor amplitudes were deposited into the Protein Data Bank with ID 3X00.

Table 3-1. Data collection and refinement statistics.

	V212-Bis-IMNtail
Data collection	
Space group	$C222_1$
Unit-cell parameters (Å, °)	a = 77.35, b = 77.38, c = 174.12
Wavelength	0.90000
Resolution (Å)	50–1.30 (1.35–1.30)[a]
R_{sym} (%)[b]	5.6 (30.4)
Total reflections	1,015,993
Unique reflections	127,145 (12,529)
$I/\sigma(I)$	35.8 (3.9)
Completeness (%)	99.6 (99.6)
Redundancy	8.0 (5.8)
Refinement	
Resolution	1.30
No. of reflections	120,725
R_{work} (%)[c]/R_{free} (%)[d]	14.6/18.8
No. of atoms	
Protein	3,863
Ligand/ion	100
Water	442
B factors	
Protein	22.0
Ligand/ion	23.7
Water	38.5
R.m.s deviations	
Bond length (Å)	0.022
Bond angles (°)	2.23
Ramachandran plot	
Favored (%)	95.48
Allowed (%)	3.85
Outliers (%)	0.68
PDB IDs	3X00

[a]Values in parentheses are for the highest-resolution shell.

[b]R_{sym} is calculated as $\Sigma_{hkl}\Sigma_i|I_i(\text{hkl}) - \langle I(hkl)\rangle|/\Sigma_{hkl}\Sigma_i I(hkl)$, where $I_i(hkl)$ is the intensity of an individual measurement of the reflection with Miller indices hkl and $\langle I(hkl)\rangle$ is the average intensity from multiple observations.

[c]$R_{work} = \Sigma_{hkl}||F_{obs}| - |F_{calc}||/\Sigma_{hkl}|F_{obs}|$, where F_{obs} and F_{calc} are the observed and calculated structure-factor amplitudes, respectively.

3.3. Results and Discussion

3.3.1. Design and synthesis of Bis-IMNtail

The binding affinity of V212 for IMNtail was relatively low compared with the original binding affinity of SA/BTN, and further modifications are necessary before it can be used practically in a pre-targeting system. To increase the binding affinity of IMNtail to V212, the author focused on the distance and orientation between the carboxylates of two IMNtail molecules bound in neighboring subunits. They seemed to be close enough (2.96 Å) to be linked by two or three additional covalent bonds (Fig. 3-1A). In previous reports (*60, 61*), a bivalent BTN analog (two BTN units connected with a linker) was shown to dramatically increase the binding affinity for SA. It is thought that the dual binding of the bivalent analog induces a striking avidity effect that leads to higher affinity, although there is no structural evidence for this hypothesis.

Based on this idea, another bivalent analog connecting two IMNtail molecules was designed and synthesized (Bis-IMNtail; Fig. 3-1B). Considering the linear distance (2.96 Å) between two IMNtails, they are connected with a -N-C-C-N- linker (the N-N distance in *trans* configuration is 3.7 Å) rather than a -N-C-N- linker (the N-N distance 2.4 Å), for the linker flexibility. SPR measurement showed that the Bis-IMNtail has a K_d value of over 8.3×10^{-10} M toward V212. This is a much higher affinity than that for the monovalent IMNtail ($K_d = 5.9\times10^{-7}$ M). Note that this K_d value was over the detection limit of the SPR assay, thus the actual affinity of V212 for Bis-IMNtail will be higher.

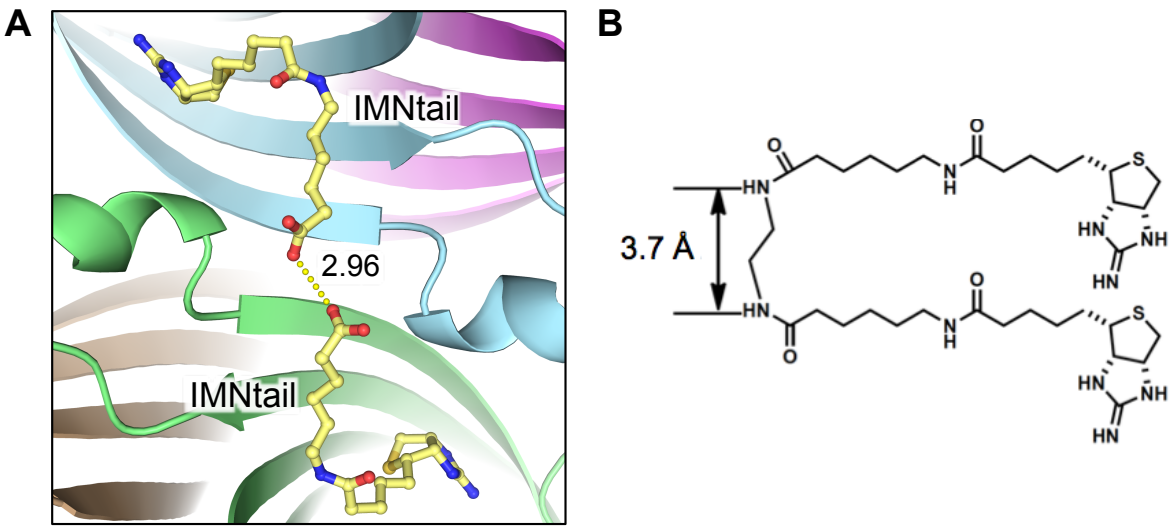

Fig. 3-1. Distance of two neighboring IMNtail molecules in V212. (A) Two IMNtail molecules are shown in stick models, and V212 subunits are drawn as ribbon models. Numbers indicate the distance (Å) between two IMNtail molecules by yellow dot line. (B) Structural formula of Bis-IMNtail.

3.3.2. Crystal structure of V212 in complex with Bis-IMNtail

To investigate the binding mode of Bis-IMNtail, the crystal structure of V212 in complex with Bis-IMNtail was solved at 1.3 Å resolution. This is the first structure of SA in complex with a bivalent ligand. V212 forms a tetramer composed of a dimer of dimers (Fig. 3-2B), the same as SA structures solved previously. As expected, two Bis-IMNtail molecules bind to the tetramer, one binding to the pocket of two neighboring protomers. The electron density map of Bis-IMNtail was clearly observed (Fig. 3-2B). The binding mode of Bis-IMNtail is well preserved in that of IMNtail complexed with V212, including the area around the connecting positions of the Bis-IMNtail (Fig. 3-2C, D). In brief, Asp23 and Asp27 form hydrogen bond with the guanidino nitrogen of Bis-IMNtail in 2.9 Å distance, and the binding loop composed of 45–52 residues forms the flexible open conformation, with no interaction with ligand. It is conceivable that designing the loop forming interactions with Bis-IMNtail may increase its affinity. As for the interaction between Asp128 and the guanidino nitogen, it is altered from interaction *via* a water molecule in the IMNtail complex to a

direct hydrogen bond in the Bis-IMNtail complex. From structural analyses, any newly-formed interactions or conformational changes that may contribute to the increased binding affinity of Bis-IMNtail were not observed. Thus, the author concludes that the main reason for the dramatically increased affinity of Bis-IMNtail for V212 is ligand bivalency and concomitant avidity.

Previous preclinical studies have shown that pre-targeting method using SA/BTN has great efficacy for cancer treatment in mice fed with biotin deficient diet, in which endogenous BTN concentration was been greatly restricted (*54, 61*). However, this method cannot be applied to human due to the high health risk of BTN deficiency, and the lack of SA binding system that avoids competitive inhibition of endogenous BTN species.

V212 can bind to non-natural BTN analog, namely Bis-IMNtail, with high affinity (K_d = 8.3 × 10^{-10} M) while showing no affinity for another BTN specie, namely biocytin. This promises that V212 can capture the Bis-IMNtail in the human body without any binding competition from endogenous BTN species. However, f course, *in vivo* efficacy of the V212/Bis-IMNtail interaction must be evaluated. In addition, the immunogenicity test of V212 with often animal models and the development of a Bis-IMNtail molecule conjugated with drugs are also needed. This V212/Bis-IMNtail high interaction without any influence from endogenous BTN species could be applicable to the pre-targeting cancer therapy as a delivery tool, and also could be useful in biotechonological applications such as an assay system using specific binding pairs.

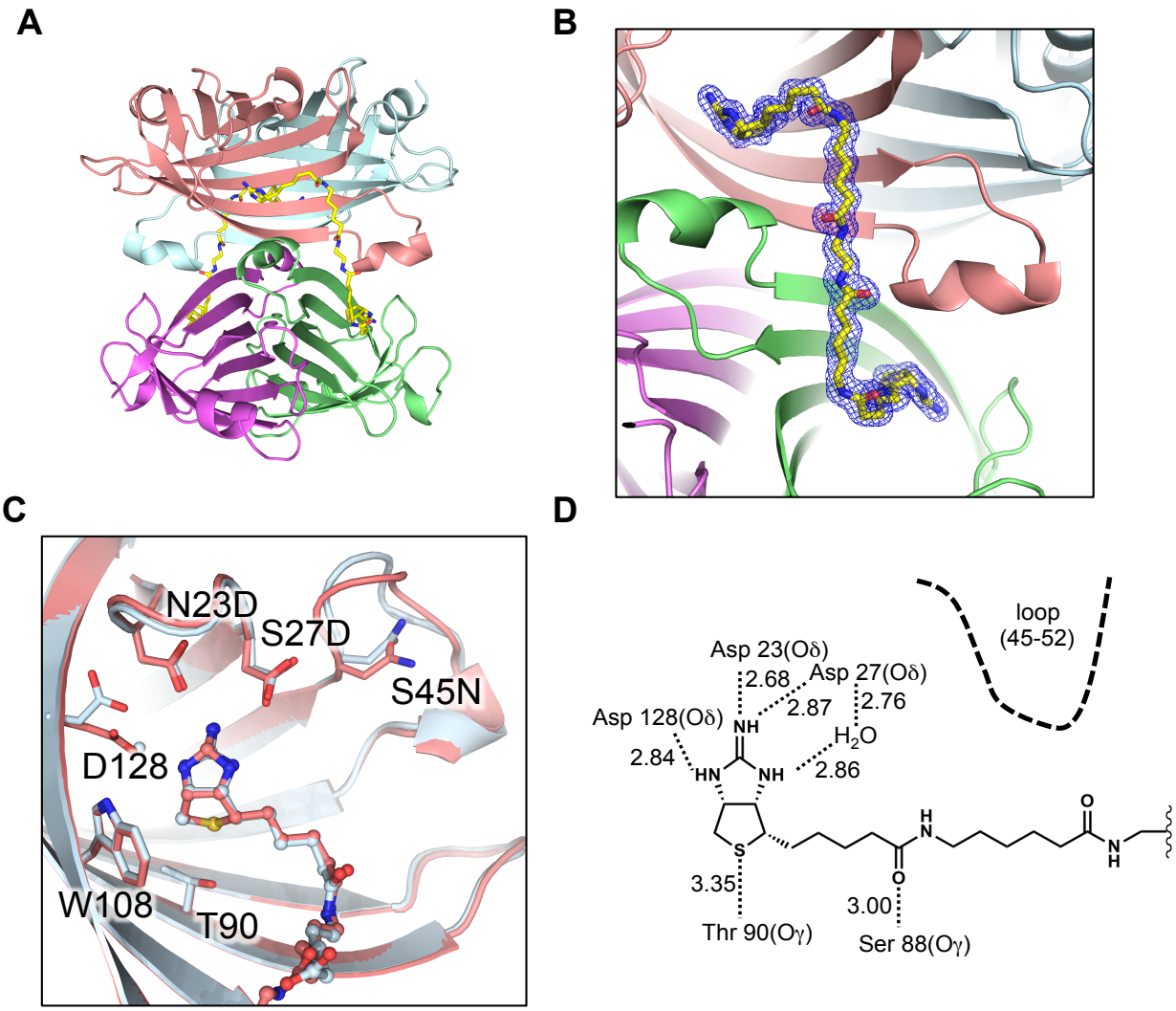

Fig. 3-2. Binding mode of Bis-IMNtail in V212. (A) Structure of the V212 tetramer (ribbon model) in complex with Bis-IMNtail (stick model). (B) The 2*F*o-*F*c electron density map of Bis-IMNtail bound to V212 is shown (blue mesh; contoured at 1.0 σ). (C) Superimposition of Bis-IMNtail-bound V212 (red) and IMNtail-bound V212 (cyan) structures is shown. (D) Schematic representations of the interactions between Bis-IMNtail and V212 are shown. The loop in V212 is presented with the dash-dot lines, because it forms an open conformation and does not interact with the ligand. The distances (Å) between amino-acid residues and Bis-IMNtail are represented by dotted lines.

3.4. Summary

In this chapter, the author developed a bivalent ligand, namely Bis-IMNtail, by connecting two IMNtail molecules in neighboring subunits in V212. Bis-IMNtail demonstrated much higher affinity (K_d = 8.3 × 10^{-10} M) toward V212 than monovalent IMNtail. This V212 and Bis-IMNtail system could be a promising technology as a novel drug delivery tool.

Conclusion

The goal of this thesis is to create a practical and bioavailable SA-binding system for the application to antibody pre-targeting method. The author carried out the molecular design of the modified LISA-314 binding system without being affected by endogenous BTN species based on X-ray structural analysis. The results obtained through this work are summarized as follows:

In chapter 1, the effects of six substitutions on the structure and function in LISA-314 were evaluated. The high-resolution crystal structure of LISA-314 revealed that LISA-314 maintains an intact tetrameric assembly, main chain frameworks, and BTN-binding mode at the same level as SA-WT. In addition, no large decrease of flexibility around the substituted sites is observed, indicating that the reduction of immunogenicity of LISA-314 is not resulted from structural changes.

Chapter 2 describes the molecular design of a modified LISA-314 binding system that avoids the influence from endogenous BTN species. By improving the binding pocket of LISA-314 through three amino acid substitutions (N23D/S27D/S45N), a modified LISA-314 mutant (V212) was developed, which binds only to a newly designed artificial BTN analogue (IMNtail, $K_d = 5.9 \times 10^{-7}$ M) and has no binding affinity for biocytin.

In chapter 3, in order to increase the affinity between V212 and IMNtail, a new ligand for V212 was developed. From the structural information of V212 complexed with IMNtail, a bivalent ligand, namely Bis-IMNtail, was designed by connecting two IMNtail molecules in neighboring subunits in V212. Bis-IMNtail demonstrated much higher affinity ($K_d = 8.3 \times 10^{-10}$ M) toward V212 than monovalent IMNtail by inducing avidity effect.

In conclusion, the author succeeded in creating a new SA-binding system, V212 and Bis-IMNtail, which displays high potential for future usage in pre-targeting method as a novel drug delivery tool.

References

(1) Bray, F., Jemal, A., Grey, N., Ferlay, J., and Forman, D. (2012) Global cancer transitions according to the Human Development Index (2008-2030): a population-based study. *Lancet Oncol.* **13**, 790-801.

(2) Siegel, R., Ma, J., Zou, Z., and Jemal, A. (2014) Cancer statistics, 2014. *CA Cancer J. Clin.* **64**, 9-29.

(3) Ferlay, J., Shin, H.R., Bray, F., Forman, D., Mathers, C., and Parkin, D.M. (2010) Estimates of worldwide burden of cancer in 2008: GLOBOCAN 2008. *Int. J. Cancer*. **127**, 2893-2917.

(4) Lu, C., and Hassan, H.T. (2006) Human stem cell factor-antibody [anti-SCF] enhances chemotherapy cytotoxicity in human CD34+ resistant myeloid leukaemia cells. *Leuk. Res.* **30**, 296-302.

(5) Reichert, J.M., and Valge-Archer, V.E. (2007) Development trends for monoclonal antibody cancer therapeutics. *Nat. Rev. Drug Discov.* **6**, 349-356.

(6) Narang, A.S., and Desai, D.S. (2009) Anticancer Drug Development. 49-92.

(7) Stern, M., and Herrmann, R. (2005) Overview of monoclonal antibodies in cancer therapy: present and promise. *Crit. Rev. Oncol. Hematol.* **54**, 11-29.

(8) Scott, A.M., Wolchok, J.D., and Old, L.J. (2012) Antibody therapy of cancer. *Nat. Rev. Cancer*. **12**, 278-287.

(9) Behring, E., and Kitasato, S. (1890) Ueber das Zustandekommen der Diphtherie-Immunitat und der Tetanus-Immunitat bei Theiren. *Deutsche. Med. Wochenschr*. **16**, 1113-1114.

(10) Weiner, L.M., Murray, J.C., and Shuptrine, C.W. (2012) Antibody-based immunotherapy of cancer. *Cell*. **148**, 1081-1084.

(11) Tansey, E.M., and Catterall, P.P. (1994) Monoclonal antibodies: a witness seminar in contemporary medical history. *Med. Hist.* **38**, 322-327.

(12) Kohler, G., and Milstein, C. (1975) Continuous cultures of fused cells secreting antibody of predefined specificity. *Nature*. **256**, 495-497.

(13) Zafir-Lavie, I., Michaeli, Y., and Reiter, Y. (2007) Novel antibodies as anticancer agents. *Oncogene*. **26**, 3714-3733.

(14) Adams, G.P., and Weiner, L.M. (2005) Monoclonal antibody therapy of cancer. *Nat. Biotechnol.* **23**, 1147-1157.

(15) Wu, A.M., and Senter, P.D. (2005) Arming antibodies: prospects and challenges for immunoconjugates. *Nat. Biotechnol.* **23**, 1137-1146.

(16) Carter, P. (2001) Improving the efficacy of antibody-based cancer therapies. *Nat. Rev. Cancer*. **1**, 118-129.

(17) Trikha, M., Yan, L., and Nakada, M.T. (2002) Monoclonal antibodies as therapeutics in oncology. *Curr. Opin. Biotechnol.* **13**, 609-614.

(18) Gelderman, K.A., Tomlinson, S., Ross, G.D., and Gorter, A. (2004) Complement function in mAb-mediated cancer immunotherapy. *Trends Immunol.* **25**, 158-164.

(19) Bruggemann, M., Williams, G.T., Bindon, C.I., Clark, M.R., Walker, M.R., Jefferis, R., Waldmann, H., and Neuberger, M.S. (1987) Comparison of the effector functions of human immunoglobulins using a matched set of chimeric antibodies. *J. Exp. Med.* **166**, 1351-1361.

(20) Wilder, R.B., DeNardo, G.L., and DeNardo, S.J. (1996) Radioimmunotherapy: recent results and future directions. *J. Clin. Oncol.* **14**, 1383-1400.

(21) Kreitman, R.J., Wilson, W.H., Bergeron, K., Raggio, M., Stetler-Stevenson, M., FitzGerald, D.J., and Pastan, I. (2001) Efficacy of the anti-CD22 recombinant immunotoxin BL22 in chemotherapy-resistant hairy-cell leukemia. *N. Engl. J. Med.* **345**, 241-247.

(22) Vogel, C.L., Cobleigh, M.A., Tripathy, D., Gutheil, J.C., Harris, L.N., Fehrenbacher, L., Slamon, D.J., Murphy, M., Novotny, W.F., Burchmore, M., Shak, S., Stewart, S.J., and Press, M. (2002) Efficacy and safety of trastuzumab as a single agent in first-line treatment of HER2-overexpressing metastatic breast cancer. *J. Clin. Oncol.* **20**, 719-726.

(23) Slamon, D.J., Leyland-Jones, B., Shak, S., Fuchs, H., Paton, V., Bajamonde, A., Fleming, T., Eiermann, W., Wolter, J., Pegram, M., Baselga, J., and Norton, L. (2001) Use of chemotherapy plus a monoclonal antibody against HER2 for metastatic breast cancer that overexpresses HER2. *N. Engl. J. Med.* **344**, 783-792.

(24) Robert, F., Ezekiel, M.P., Spencer, S.A., Meredith, R.F., Bonner, J.A., Khazaeli, M.B., Saleh, M.N., Carey, D., LoBuglio, A.F., Wheeler, R.H., Cooper, M.R., and Waksal, H.W. (2001) Phase I study of anti--epidermal growth factor receptor antibody cetuximab in combination with radiation therapy in patients with advanced head and neck cancer. *J. Clin. Oncol.* **19**, 3234-3243.

(25) Witzig, T.E., Gordon, L.I., Cabanillas, F., Czuczman, M.S., Emmanouilides, C., Joyce, R., Pohlman, B.L., Bartlett, N.L., Wiseman, G.A., Padre, N., Grillo-Lopez, A.J., Multani, P., and White, C.A. (2002) Randomized controlled trial of yttrium-90-labeled ibritumomab tiuxetan radioimmunotherapy versus rituximab immunotherapy for patients with relapsed or refractory low-grade, follicular, or transformed B-cell non-Hodgkin's lymphoma. *J. Clin. Oncol.* **20**, 2453-2463.

(26) Davis, T.A., Kaminski, M.S., Leonard, J.P., Hsu, F.J., Wilkinson, M., Zelenetz, A., Wahl, R.L., Kroll, S., Coleman, M., Goris, M., Levy, R., and Knox, S.J. (2004) The radioisotope contributes significantly to the activity of radioimmunotherapy. *Clin. Cancer Res.* **10**, 7792-7798.

(27) Goldenberg, D.M., Sharkey, R.M., Paganelli, G., Barbet, J., and Chatal, J.F. (2006) Antibody pretargeting advances cancer radioimmunodetection and radioimmunotherapy. *J. Clin. Oncol.* **24**, 823-834.

(28) Sharkey, R.M., and Goldenberg, D.M. (2005) Perspectives on cancer therapy with radiolabeled monoclonal antibodies. *J. Nucl. Med.* **46 Suppl 1**, 115s-127s.

(29) Goldenberg, D.M. (2002) Targeted therapy of cancer with radiolabeled antibodies. *J. Nucl. Med.* **43**, 693-713.

(30) Schubiger, P.A., Alberto, R., and Smith, A. (1996) Vehicles, chelators, and radionuclides: choosing the "building blocks" of an effective therapeutic radioimmunoconjugate. *Bioconjug. Chem.* **7**, 165-179.

(31) Milenic, D.E., Brady, E.D., and Brechbiel, M.W. (2004) Antibody-targeted radiation cancer therapy. *Nat. Rev. Drug Discov.* **3**, 488-499.

(32) Jhanwar, Y.S., and Divgi, C. (2005) Current status of therapy of solid tumors. *J. Nucl. Med.* **46 Suppl 1**, 141s-150s.

(33) Forero, A., Weiden, P.L., Vose, J.M., Knox, S.J., LoBuglio, A.F., Hankins, J., Goris, M.L., Picozzi, V.J., Axworthy, D.B., Breitz, H.B., Sims, R.B., Ghalie, R.G., Shen, S., and Meredith, R.F. (2004) Phase 1 trial of a novel anti-CD20 fusion protein in pretargeted radioimmunotherapy for B-cell non-Hodgkin lymphoma. *Blood*. **104**, 227-236.

(34) Press, O.W., Eary, J.F., Appelbaum, F.R., Martin, P.J., Badger, C.C., Nelp, W.B., Glenn, S., Butchko, G., Fisher, D., Porter, B., and et al. (1993) Radiolabeled-antibody therapy of B-cell

lymphoma with autologous bone marrow support. *N. Engl. J. Med.* **329**, 1219-1224.

(35) Press, O.W., Eary, J.F., Gooley, T., Gopal, A.K., Liu, S., Rajendran, J.G., Maloney, D.G., Petersdorf, S., Bush, S.A., Durack, L.D., Martin, P.J., Fisher, D.R., Wood, B., Borrow, J.W., Porter, B., Smith, J.P., Matthews, D.C., Appelbaum, F.R., and Bernstein, I.D. (2000) A phase I/II trial of iodine-131-tositumomab (anti-CD20), etoposide, cyclophosphamide, and autologous stem cell transplantation for relapsed B-cell lymphomas. *Blood*. **96**, 2934-2942.

(36) Frampas, E., Rousseau, C., Bodet-Milin, C., Barbet, J., Chatal, J.F., and Kraeber-Bodere, F. (2013) Improvement of radioimmunotherapy using pretargeting. *Front. Oncol.* **3**, 159.

(37) Goodwin, D., Meares, C., Diamanti, C., McCall, M., Lai, C., Torti, F., McTigue, M., and Martin, B. (1984) Use of specific antibody for rapid clearance of circulating blood background from radiolabeled tumor imaging proteins. *Eur. J. Nucl. Med.* **9**, 209-215.

(38) Green, D.J., Orgun, N.N., Jones, J.C., Hylarides, M.D., Pagel, J.M., Hamlin, D.K., Wilbur, D.S., Lin, Y., Fisher, D.R., Kenoyer, A.L., Frayo, S.L., Gopal, A.K., Orozco, J.J., Gooley, T.A., Wood, B.L., Bensinger, W.I., and Press, O.W. (2014) A preclinical model of CD38-pretargeted radioimmunotherapy for plasma cell malignancies. *Cancer Res.* **74**, 1179-1189.

(39) Boerman, O.C., van Schaijk, F.G., Oyen, W.J., and Corstens, F.H. (2003) Pretargeted radioimmunotherapy of cancer: progress step by step. *J. Nucl. Med.* **44**, 400-411.

(40) Palanca-Wessels, M.C., and Press, O.W. (2014) Advances in the treatment of hematologic malignancies using immunoconjugates. *Blood*. **123**, 2293-2301.

(41) Press, O.W., Corcoran, M., Subbiah, K., Hamlin, D.K., Wilbur, D.S., Johnson, T., Theodore, L., Yau, E., Mallett, R., Meyer, D.L., and Axworthy, D. (2001) A comparative evaluation of conventional and pretargeted radioimmunotherapy of CD20-expressing lymphoma xenografts. *Blood*. **98**, 2535-2543.

(42) Pagel, J.M., Hedin, N., Subbiah, K., Meyer, D., Mallet, R., Axworthy, D., Theodore, L.J., Wilbur, D.S., Matthews, D.C., and Press, O.W. (2003) Comparison of anti-CD20 and anti-CD45 antibodies for conventional and pretargeted radioimmunotherapy of B-cell lymphomas. *Blood*. **101**, 2340-2348.

(43) Pantelias, A., Pagel, J.M., Hedin, N., Saganic, L., Wilbur, S., Hamlin, D.K., Wilbur, D.S., Lin, Y., Stone, D., Axworthy, D., Gopal, A.K., and Press, O.W. (2007) Comparative biodistributions of pretargeted radioimmunoconjugates targeting CD20, CD22, and DR molecules on human B-cell lymphomas. *Blood*. **109**, 4980-4987.

(44) Axworthy, D.B., Reno, J.M., Hylarides, M.D., Mallett, R.W., Theodore, L.J., Gustavson, L.M., Su, F., Hobson, L.J., Beaumier, P.L., and Fritzberg, A.R. (2000) Cure of human carcinoma xenografts by a single dose of pretargeted yttrium-90 with negligible toxicity. *Proc. Natl. Acad. Sci. U. S. A.* **97**, 1802-1807.

(45) Zhang, M., Zhang, Z., Garmestani, K., Schultz, J., Axworthy, D.B., Goldman, C.K., Brechbiel, M.W., Carrasquillo, J.A., and Waldmann, T.A. (2003) Pretarget radiotherapy with an anti-CD25 antibody-streptavidin fusion protein was effective in therapy of leukemia/lymphoma xenografts. *Proc. Natl. Acad. Sci. U. S. A.* **100**, 1891-1895.

(46) Green, N.M. (1975) Avidin. *Adv. Protein Chem.* **29**, 85-133.

(47) Chaiet, L., and Wolf, F.J. (1964) THE PROPERTIES OF STREPTAVIDIN, A BIOTIN-BINDING PROTEIN PRODUCED BY STREPTOMYCETES. *Arch. Biochem. Biophys.* **106**, 1-5.

(48) Diamandis, E.P., and Christopoulos, T.K. (1991) The biotin-(strept)avidin system: principles and applications in biotechnology. *Clin. Chem.* **37**, 625-636.

(49) Voss, S., and Skerra, A. (1997) Mutagenesis of a flexible loop in streptavidin leads to higher affinity for the Strep-tag II peptide and improved performance in recombinant protein purification. *Protein Eng.* **10**, 975-982.

(50) Korndorfer, I.P., and Skerra, A. (2002) Improved affinity of engineered streptavidin for the Strep-tag II peptide is due to a fixed open conformation of the lid-like loop at the binding site. *Protein Sci.* **11**, 883-893.

(51) Schmidt, T.G., and Skerra, A. (2007) The Strep-tag system for one-step purification and high-affinity detection or capturing of proteins. *Nat. Protoc.* **2**, 1528-1535.

(52) Chang, C.H., Sharkey, R.M., Rossi, E.A., Karacay, H., McBride, W., Hansen, H.J., Chatal, J.F., Barbet, J., and Goldenberg, D.M. (2002) Molecular advances in pretargeting radioimunotherapy with bispecific antibodies. *Mol. Cancer Ther.* **1**, 553-563.

(53) Meyer, D.L., Schultz, J., Lin, Y., Henry, A., Sanderson, J., Jackson, J.M., Goshorn, S., Rees, A.R., and Graves, S.S. (2001) Reduced antibody response to streptavidin through site-directed mutagenesis. *Protein Sci.* **10**, 491-503.

(54) Pagel, J.M., Matthews, D.C., Kenoyer, A., Hamlin, D.K., Wilbur, D.S., Fisher, D.R., Gopal, A.K., Lin, Y., Saganic, L., Appelbaum, F.R., and Press, O.W. (2009) Pretargeted radioimmunotherapy using anti-CD45 monoclonal antibodies to deliver radiation to murine hematolymphoid tissues and human myeloid leukemia. *Cancer Res.* **69**, 185-192.

(55) Paganelli, G., Chinol, M., Maggiolo, M., Sidoli, A., Corti, A., Baroni, S., and Siccardi, A.G. (1997) The three-step pretargeting approach reduces the human anti-mouse antibody response in patients submitted to radioimmunoscintigraphy and radioimmunotherapy. *Eur. J. Nucl. Med.* **24**, 350-351.

(56) Forster, G.J., Santos, E.B., Smith-Jones, P.M., Zanzonico, P., and Larson, S.M. (2006) Pretargeted radioimmunotherapy with a single-chain antibody/streptavidin construct and radiolabeled DOTA-biotin: strategies for reduction of the renal dose. *J. Nucl. Med.* **47**, 140-149.

(57) Baker, H. (1985) Assessment of biotin status: clinical implications. *Ann. N. Y. Acad. Sci.* **447**, 129-132.

(58) Knox, S.J., Goris, M.L., Tempero, M., Weiden, P.L., Gentner, L., Breitz, H., Adams, G.P., Axworthy, D., Gaffigan, S., Bryan, K., Fisher, D.R., Colcher, D., Horak, I.D., and Weiner, L.M. (2000) Phase II trial of yttrium-90-DOTA-biotin pretargeted by NR-LU-10 antibody/streptavidin in patients with metastatic colon cancer. *Clin. Cancer Res.* **6**, 406-414.

(59) Reznik, G.O., Vajda, S., Sano, T., and Cantor, C.R. (1998) A streptavidin mutant with altered ligand-binding specificity. *Proc. Natl. Acad. Sci. U. S. A.* **95**, 13525-13530.

(60) Hamblett, K.J., Kegley, B.B., Hamlin, D.K., Chyan, M.K., Hyre, D.E., Press, O.W., Wilbur, D.S., and Stayton, P.S. (2002) A streptavidin-biotin binding system that minimizes blocking by endogenous biotin. *Bioconjug. Chem.* **13**, 588-598.

(61) Park, S.I., Shenoi, J., Frayo, S.M., Hamlin, D.K., Lin, Y., Wilbur, D.S., Stayton, P.S., Orgun, N., Hylarides, M., Buchegger, F., Kenoyer, A.L., Axtman, A., Gopal, A.K., Green, D.J., Pagel, J.M., and Press, O.W. (2011) Pretargeted radioimmunotherapy using genetically engineered antibody-streptavidin fusion proteins for treatment of non-hodgkin lymphoma. *Clin. Cancer Res.* **17**, 7373-7382.

(62) Kodama, T., Hamakubo, T., Sugiyama, A., and Tsumoto, K. (2010) Hypo-immunogenic streptavidin and use thereof. International Patent Application. *In ternational Patent Application*. **WO/2010/095455**.

(63) Yumura, K., Ui, M., Doi, H., Hamakubo, T., Kodama, T., Tsumoto, K., and Sugiyama, A.

(2013) Mutations for decreasing the immunogenicity and maintaining the function of core streptavidin. *Protein Sci.* **22**, 213-221.

(64) McCoy, A.J., Grosse-Kunstleve, R.W., Adams, P.D., Winn, M.D., Storoni, L.C., and Read, R.J. (2007) Phaser crystallographic software. *J Appl Crystallogr*. **40**, 658-674.

(65) (1994) The CCP4 suite: programs for protein crystallography. *Acta Crystallogr. D Biol. Crystallogr.* **50**, 760-763.

(66) Emsley, P., Lohkamp, B., Scott, W.G., and Cowtan, K. (2010) Features and development of Coot. *Acta Crystallogr. D Biol. Crystallogr.* **66**, 486-501.

(67) Murshudov, G.N., Vagin, A.A., and Dodson, E.J. (1997) Refinement of macromolecular structures by the maximum-likelihood method. *Acta Crystallogr. D Biol. Crystallogr.* **53**, 240-255.

(68) Weber, P.C., Wendoloski, J.J., Pantoliano, M.W., and Salemme, F.R. (1992) Crystallographic and thermodynamic comparison of natural and synthetic ligands bound to streptavidin. *J. Am. Chem. Soc.* **114**, 3197-3200.

(69) Pahler, A., Hendrickson, W.A., Kolks, M.A., Argarana, C.E., and Cantor, C.R. (1987) Characterization and crystallization of core streptavidin. *J. Biol. Chem.* **262**, 13933-13937.

(70) Freitag, S., Le Trong, I., Klumb, L., Stayton, P.S., and Stenkamp, R.E. (1997) Structural studies of the streptavidin binding loop. *Protein Sci.* **6**, 1157-1166.

(71) Hyre, D.E., Le Trong, I., Merritt, E.A., Eccleston, J.F., Green, N.M., Stenkamp, R.E., and Stayton, P.S. (2006) Cooperative hydrogen bond interactions in the streptavidin-biotin system. *Protein Sci.* **15**, 459-467.

(72) Hyre, D.E., Le Trong, I., Freitag, S., Stenkamp, R.E., and Stayton, P.S. (2000) Ser45 plays an important role in managing both the equilibrium and transition state energetics of the streptavidin-biotin system. *Protein Sci.* **9**, 878-885.

(73) Le Trong, I., Wang, Z., Hyre, D.E., Lybrand, T.P., Stayton, P.S., and Stenkamp, R.E. (2011) Streptavidin and its biotin complex at atomic resolution. *Acta Crystallogr. D Biol. Crystallogr.* **67**, 813-821.

(74) Hytonen, V.P., Maatta, J.A., Niskanen, E.A., Huuskonen, J., Helttunen, K.J., Halling, K.K., Nordlund, H.R., Rissanen, K., Johnson, M.S., Salminen, T.A., Kulomaa, M.S., Laitinen, O.H., and Airenne, T.T. (2007) Structure and characterization of a novel chicken biotin-binding protein A (BBP-A). *BMC Struct. Biol.* **7**, 8.

(75) Baugh, L., Le Trong, I., Cerutti, D.S., Mehta, N., Gulich, S., Stayton, P.S., Stenkamp, R.E., and Lybrand, T.P. (2012) Second-contact shell mutation diminishes streptavidin-biotin binding affinity through transmitted effects on equilibrium dynamics. *Biochemistry*. **51**, 597-607.

(76) Karplus, P.A., and Schulz, G.E. (1985) Prediction of chain flexibility in proteins. *Naturwissenschaften*. **72**, 212-213.

(77) Gallizia, A., de Lalla, C., Nardone, E., Santambrogio, P., Brandazza, A., Sidoli, A., and Arosio, P. (1998) Production of a soluble and functional recombinant streptavidin in Escherichia coli. *Protein Expr. Purif.* **14**, 192-196.

(78) Sano, T., and Cantor, C.R. (1995) Intersubunit contacts made by tryptophan 120 with biotin are essential for both strong biotin binding and biotin-induced tighter subunit association of streptavidin. *Proc. Natl. Acad. Sci. U. S. A.* **92**, 3180-3184.

(79) Sano, T., and Cantor, C.R. (1990) Expression of a cloned streptavidin gene in Escherichia coli. *Proc. Natl. Acad. Sci. U. S. A.* **87**, 142-146.

(80) Thompson, L.D., and Weber, P.C. (1993) Construction and expression of a synthetic

streptavidin-encoding gene in Escherichia coli. *Gene*. **136**, 243-246.

(81) Kawato, T., Mizohata, E., Shimizu, Y., Meshizuka, T., Yamamoto, T., Takasu, N., Matsuoka, M., Matsumura, H., Kodama, T., Kanai, M., Doi, H., Inoue, T., and Sugiyama, A. Structure-based design of a streptavidin mutant specific for an artificial biotin analog. *The Journal of Biochemistry*.

(82) Kawato, T., Mizohata, E., Meshizuka, T., Doi, H., Kawamura, T., Matsumura, H., Yumura, K., Tsumoto, K., Kodama, T., Inoue, T., and Sugiyama, A. (2014) Crystal structure of streptavidin mutant with low immunogenicity. *J. Biosci. Bioeng.*,

(83) Stayton, P.S., Freitag, S., Klumb, L.A., Chilkoti, A., Chu, V., Penzotti, J.E., To, R., Hyre, D., Le Trong, I., Lybrand, T.P., and Stenkamp, R.E. (1999) Streptavidin-biotin binding energetics. *Biomol. Eng.* **16**, 39-44.

(84) Athappilly, F.K., and Hendrickson, W.A. (1997) Crystallographic analysis of the pH-dependent binding of iminobiotin by streptavidin. *Protein Sci.* **6**, 1338-1342.

(85) Wilbur, D.S., Hamlin, D.K., Pathare, P.M., and Weerawarna, S.A. (1997) Biotin reagents for antibody pretargeting. Synthesis, radioiodination, and in vitro evaluation of water soluble, biotinidase resistant biotin derivatives. *Bioconjug. Chem.* **8**, 572-584.

(86) Weber, P.C., Ohlendorf, D.H., Wendoloski, J.J., and Salemme, F.R. (1989) Structural origins of high-affinity biotin binding to streptavidin. *Science*. **243**, 85-88.

(87) Kawato, T., Mizohata, E., Shimizu, Y., Meshizuka, T., Yamamoto, T., Takasu, N., Matsuoka, M., Matsumura, H., Kodama, T., Kanai, M., Doi, H., Inoue, T., and Sugiyama, A. Structure-based design and synthesis of a bivalent iminobiotin analog showing strong affinity toward a low immunogenic streptavidin mutant. *Biosci., Biotechnol., Biochem.*, in press.

List of Publications

1. Crystal Structure of a Streptavidin Mutant with Low Immunogenicity

Tatsuya Kawato, Eiichi Mizohata, Tomohiro Meshizuka, Hirofumi Doi, Takeshi Kawamura, Hiroyoshi Matsumura, Kyohei Yumura, Kouhei Tsumoto, Tatsuhiko Kodama, Tsuyoshi Inoue & Akira Sugiyama

J. of Biosci. and Bioeng., in press.

2. Structure-based design and synthesis of a bivalent iminobiotin analog showing strong affinity toward a low immunogenic streptavidin mutant

Tatsuya Kawato, Eiichi Mizohata, Yohei Shimizu, Tomohiro Meshizuka, Tomohiro Yamamoto, Noriaki Takasu, Masahiro Matsuoka, Hiroyoshi Matsumura, Tatsuhiko Kodama, Motomu Kanai, Hirofumi Doi, Tsuyoshi Inoue & Akira Sugiyama

Bioscience, Biotechnology, and Biochemistry, in press.

3. Structure-based design of a streptavidin mutant specific for an artificial biotin analog

Tatsuya Kawato, Eiichi Mizohata, Yohei Shimizu, Tomohiro Meshizuka, Tomohiro Yamamoto, Noriaki Takasu, Masahiro Matsuoka, Hiroyoshi Matsumura, Tatsuhiko Kodama, Motomu Kanai, Hirofumi Doi, Tsuyoshi Inoue & Akira Sugiyama

The Journal of Biochemistry, in press.

Acknowledgements

The author would like to express his heartfelt gratitude to Professor Dr. Tsuyoshi Inoue, Department of Applied Chemistry, Graduate School of Engineering, Osaka University, for his continuous guidance, many invaluable suggestions, and his science encouragement throughout the work. The author is indebted to Dr. Eiichi Mizohata, Department of Applied Chemistry, Graduate School of Engineering, Osaka University, for his continuous guidance and stimulating discussions for carrying out this work. The author is also very grateful to Dr. Hiroyoshi Matsumura, Department of Applied Chemistry, Graduate School of Engineering, Osaka University, for his helpful suggestions and heartfelt advice.

The author acknowledges to Professor Dr. Hiroshi Uyama and Professor Dr. Takashi Hayashi for reviewing this thesis and giving their valuable comments.

It should be emphasized that the studies in this thesis have required the cooperation with a number of groups of investigation. The author desires to express his sincere thanks to Professor Dr. Tatsuhiko Kodama and Professor Dr. Hirofumi Doi, Research Center for Advanced Science and Technology, The University of Tokyo, for their helpful suggestions and heartfelt advice.

The author is deeply grateful to Dr. Akira Sugiyama, Radioisotope Center, The University of Tokyo, for his valuable suggestions for molecular design and for the SPR measurement. The author is also very grateful to Prof. Dr. Motomu Kanai and Dr. Yohei Shimizu, Graduate School of Pharmaceutical Sciences, The University of Tokyo, for the synthesis of compounds.

The author would like to thank Professor Dr. Atsushi Nakagawa, Dr. Mamoru Suzuki, Dr. Masato Yoshimura and Dr. Eiki Yamashita, beamline BL44XU at SPring-8, and Dr. Naohiro

Matsugaki and Dr. Yusuke Yamada, beamline BL17A at Photon Factory for their support in the collection of X-ray data.

Special thanks should be given to Mr. Tomohiro Meshizuka for his helpful assistance and support in the course of this work. Acknowledgement is also made to all members of Professor Dr. Tsuyoshi Inoue's lab (from April 2010 to March 2015).

Finally, the author would like to express great gratitude to his family for their unfailing understanding and affectionate encouragement.